Macrophage Inflammasome Activation Drives Anti-inflammatory Responses via Neutrophil-Derived ASC Speck Transfer and Gasdermin-Dependent Caspase-1 Inhibition

Annamaria Pedoto[1,2,3,*], Juan M. Lozano Gil[1,2,3,*], Mai E. Nguyen-Chi[4], Georges Lutfalla[4], Diana García-Moreno[2,3], Victoriano Mulero[1,2,3,#], Sylwia D. Tyrkalska[2,3,#]

[1] Departamento de Biología Celular e Histología, Facultad de Biología, Universidad de Murcia, 30100 Murcia, Spain

[2] Instituto Murciano de Investigación Biosanitaria Pascual Parrilla, 30120 Murcia, Spain.

[3] Centro de Investigación Biomédica en Red de Enfermedades Raras (CIBERER), Instituto de Salud Carlos III, 28029 Madrid, Spain.

[4] LPHI, University of Montpellier, CNRS, Montpellier, France.

*These authors contributed equally.

[#]Corresponding authors.

ABSTRACT

Inflammasomes are critical components of the innate immune system, traditionally associated with pro-inflammatory responses. While the inflammasome in macrophages has been extensively studied and linked to pyroptosis and cytokine release, the neutrophil inflammasome remains poorly understood. Neutrophil inflammasome activation drives unique outcomes such as NETosis and robust IL-1β production without inducing pyroptosis. In contrast, macrophage inflammasome activation promotes pyroptosis and the release of cytokines like IL-1α and IL-18. Here, using zebrafish models of Salmonella enterica serovar Typhimurium infection and COVID-19-associated cytokine storm syndrome (CSS), we reveal opposing roles of neutrophil and macrophage inflammasomes: neutrophil inflammasomes are pro-inflammatory, whereas macrophage inflammasomes mediate anti-inflammatory responses. We show that Gasdermin E (Gsdme)- and Ninjurin-1-mediated cell death in neutrophils releases ASC specks, which are taken up by macrophages. This transfer negatively regulates caspase-1 activity via the Gsdme, promoting the resolution of inflammation. To our knowledge, this is the first study to reveal the anti-inflammatory role of the macrophage inflammasome, document the in vivo transfer of ASC specks between neutrophils and macrophages, and uncover the negative feedback regulation of the inflammasome by the Gsdme. These results offer novel insights into potential therapeutic approaches for hyperinflammatory diseases like bacterial infections and COVID-19-associated CSS.

KEY WORDS

Inflammasome, neutrophils, macrophages, gasdermin, zebrafish

INTRODUCTION

The inflammasomes are multiprotein complexes situated in the cytosol of the immune cells, mostly macrophages, neutrophils and dendritic cells, that are crucially involved for the activation of the inflammatory response and cell death (Fu et al., 2024). They typically consist of a sensor protein, the adaptor protein apoptosis-associated speck-like protein containing a caspase-recruitment domain (ASC), and the proinflammatory caspase, caspase-1 (Nambayan et al., 2019; Schroder and Tschopp, 2010). Assembly of the inflammasome is a well-organized process comprising an inflammatory signaling cascade. It can be triggered by recognizing of a variety of stimuli that are associated with infection or cellular stress (Latz et al., 2013). Inflammasome assembly requires homotypic CARD–CARD or PYD–PYD interactions between its components inducing oligomerization (Cai et al., 2014; Lu et al., 2014). When the ligand is being detected, the sensor is relieved from an inhibitory state and recruits ASC to form a multimeric complex called speck. The sensor protein can include NLRs, AIM2 or pyrin depending on the type of danger signal involved in the process and they are categorized based on their structural characteristics (Mariathasan and Monack, 2007). Then, ASC recruits procaspase-1 (proCASP1) into the complex, which next is converted into active CASP1 that cleaves pro-IL-1β and pro-IL-18 to active cytokines and activate pore-forming Gasdermin D (GSDMD) to induce a form of a programmed cell death called pyroptosis (Van Gorp et al., 2019; Wang et al., 2021). Moreover, it has been shown that activation of the inflammasome can lead to the generation of an eicosanoid storm through the induction of cytosolic phospholipase A2 (PLA2) in resident peritoneal macrophages or neutrophils (Tyrkalska et al., 2016; von Moltke et al., 2012).

Neutrophils and macrophages are key innate immune cells that form the first line of defense against pathogens (Lendeckel et al., 2022; Su et al., 2020). Neutrophils, which constitute ~70% of circulating leukocytes, are rapidly recruited to inflammation sites, where they eliminate microbes through phagocytosis, degranulation, and the release of neutrophil extracellular traps (NETs) (Hickey and Kubes, 2009; Kolaczkowska and Kubes, 2013; Tyrkalska et al., 2021). In contrast, macrophages reside in tissues, where they clear debris and regulate inflammation (Varol et al., 2015). These cells can polarize into two main subsets: pro-inflammatory M1 macrophages and anti-inflammatory M2 macrophages, with their balance being critical for resolving inflammation and tissue repair (Shapouri-Moghaddam et al., 2018). Although both neutrophils and macrophages express functional inflammasomes, the neutrophil inflammasome remains largely understudied. Historically, inflammasome activation and IL-1β production were primarily attributed to macrophages and dendritic cells, with neutrophils considered passive recipients of pro-inflammatory cytokines (Tyrkalska et al., 2021). However, recent studies have revealed that neutrophils can activate NLRP3, NLRC4, and NLRP12

inflammasomes during bacterial infections (Chen et al., 2014; Thomas and Schroder, 2013). However, the inflammasome activation in macrophages and neutrophils leads to distinct outcomes, highlighting their functional differences. In macrophages, activation of the inflammasome causes pyroptosis, whereas in neutrophils, inflammasome activation results in GSDMD-induced formation of antimicrobial NETs and neutrophil NETosis (Chen et al., 2018; Sollberger et al., 2018; Tyrkalska et al., 2021). In addition, the resistance of neutrophils to pyroptotic cell death enables them to sustain IL-1β and eicosanoid production during bacterial infections (Chen et al., 2014; Tyrkalska et al., 2016). This difference may be linked to the size and distribution of ASC specks: neutrophils contain multiple specks per cell, while macrophages have individual specks (Boucher et al., 2018; Latz et al., 2013). Additionally, in neutrophils, inflammasome activation primarily triggers IL-1β production, while in macrophages, it induces IL-1β release alongside other cytokines, such as IL-1α and IL-18 (Bakele et al., 2014). Furthermore, while CASP1 is abundant in macrophages and drives IL-1β cleavage, in neutrophils, IL-1β cleavage is primarily mediated by serine proteases (Boucher et al., 2018). Interestingly, neutrophils can also secrete IL-1β via an autophagy-dependent mechanism (Karmakar et al., 2020). GBPs play a central role in inflammasome activation, IL-1β production, and pyroptosis in macrophages, while they are involved only in prostaglandin biosynthesis and release in neutrophils (Shenoy et al., 2012; Tyrkalska et al., 2016). Finally, the release of inflammasome components also differs: macrophages expel ASC specks into the extracellular space during pyroptosis (Baroja-Mazo et al., 2014; Franklin et al., 2014), while neutrophils secrete vesicles containing inflammasome components (Forrest et al., 2022), which amplify the inflammatory response. These findings underline the distinct roles of inflammasomes in neutrophils and macrophages, emphasizing the cell-specific mechanisms that drive immune responses.

Despite the characterization of inflammasomes in both neutrophils and macrophages, all known inflammasomes to date are associated with pro-inflammatory responses, with no reported anti-inflammatory activity. Furthermore, little is known about the interactions between neutrophil and macrophage inflammasomes, especially in terms of how they may influence each other in the context of immune responses. Using the zebrafish model, here we report that inflammasomes exhibit opposing functions in these cell types: pro-inflammatory in neutrophils and anti-inflammatory in macrophages. Remarkably, specks released from neutrophils through Gasdermin E (Gsdme)- and Ninjurin-1-mediated cell death are taken up by macrophages, where they drive an anti-inflammatory response via the C-terminal Gsdme-mediated inhibition of caspase-1 activity. To our knowledge, this is the first study to reveal the anti-inflammatory role of the macrophage inflammasome, document the in vivo transfer of ASC specks between

113 neutrophils and macrophages, and uncover the negative feedback regulation of the
114 inflammasome by the C-terminal domain of Gsdme.
115
116 **RESULTS**
117 *Inhibition of the macrophage inflammasome exacerbates inflammation in a COVID19-*
118 *associated CSS model*
119 Using a COVID-19-associated cytokine storm syndrome (CSS) model, we injected
120 recombinant S1 domain of the SARS-CoV-2 Spike protein (S1WT) into the hindbrain ventricle
121 (HBV) of 2 days post-fertilization (dpf) zebrafish larvae, as previously described larvae
122 (Tyrkalska et al., 2022; Tyrkalska et al., 2023a). To assess the number of *tnfa*$^+$ neutrophils (N1-
123 like) and macrophages (M1-like), we employed the reporter line *Tg(tnfa:GFP)*, crossed with
124 either *Tg(lyz:dsRed2)* for neutrophils or *Tg(mpeg1:mCherry)* for macrophages, allowing the
125 identification of double-positive cells. Our analysis revealed no significant differences in the
126 number of *tnfa*$^+$ neutrophils between control larvae injected with water and those injected with
127 S1WT, both in the whole body and around the injection site (head region) (Figures 1A-1B and
128 S1A-S1B). However, larvae injected with S1WT displayed a higher percentage of *tnfa*$^+$
129 macrophages, both in the whole body and specifically in the head region, compared to controls
130 (Figures 1C-1D and S1C-S1D). Despite this increase, the proportion of *tnfa*$^+$ macrophages
131 among all macrophages remained relatively low, reaching approximately 15% in the head and
132 10% in the whole body of S1WT-injected larvae."
133 We next ablated either neutrophils or macrophages, to check the role of each cell type
134 on the inflammatory response. For that we used the GAL4-UAS system by crossing two
135 different zebrafish transgenic lines: *Tg(uas:nfsB-mCherry)* and *Tg(mpx:gal4)* for neutrophils or
136 *Tg(mpeg1:gal4)* for macrophages. These fish expressed bacterial nitroreductase in cell specific
137 manner, that was able to metabolize metronidazole (MTZ) and killed the cells of interest. As
138 we expected, S1WT-injected larvae that lacked neutrophils showed decreased levels of *il1b* and
139 *tnfa* mRNA than the S1WT-injected control fish (Figures 1E-1F). Neutrophil ablation resulted
140 in increased number of macrophages (Figure 1G). In sharp contrast, S1WT-injected larvae
141 lacking macrophages showed increased levels of *il1b* and *tnfa* transcripts than S1WT-injected
142 control fish (Figures 1H-1I). As observed before, genetic ablation of macrophages resulted in
143 an increased number of neutrophils (Figure 1J).
144 To check whether these effects were mediated by cell specific inflammasome activity,
145 we then inhibited the inflammasome in either neutrophils or macrophages by overexpressing a
146 DN form of Asc lacking its CARD domain using GAL4-UAS system (Tyrkalska et al., 2019).
147 Surprisingly, we obtained the same result seen by the depletion of neutrophils and macrophages
148 (Figures 1E-1I), namely inhibition of the inflammasome in neutrophils led to attenuated S1WT-

149 induced inflammation, assayed as the mRNA levels of *il1b* and *tnfa* (Figures 1K-1L). On the
150 contrary, S1WT injected fish with inhibited inflammasome in macrophages showed increased
151 inflammation compared with their wildtype siblings (Figures 1M-1N). We then performed
152 caspase-1 activity assays as a readout of inflammasome activation. In both cases overexpression
153 of DN-Asc in either neutrophils or macrophages led to decreased systemic and local caspase-1
154 activity in both controls and inflammation conditions (Figures 1O-1R). As expected, S1WT-
155 injected larvae showed increased caspase-1 activity but, unexpectedly, inhibition of
156 macrophage inflammasome resulted in much lower caspase-1 activity levels than inhibition of
157 neutrophil inflammasome (Figure 1O-R). This result suggests that macrophages show higher
158 inflammasome activity than neutrophils in zebrafish.
159 Finally, we checked the number of cells of interest upon inhibition of either macrophage
160 or neutrophil inflammasomes. Inhibition of macrophage inflammasome resulted in increased
161 macrophage recruitment to S1WT (Figures 1S and S1E) and monocytosis in both basal and
162 inflammation conditions (Figures 1T-1U and S1F). In contrast, although the recruitment of
163 neutrophils to S1WT was unaffected upon inhibition of the neutrophil inflammasome in basal
164 and inflammatory conditions (Figure 1W and S1G), neutrophilia was apparent in larvae upon
165 inhibition of neutrophil inflammasome in basal and inflammatory conditions (Figures 1X-1Y
166 and S1H). These results suggest that both macrophages and neutrophils are clearer from
167 zebrafish larvae by pyroptosis.
168
169 *Inhibition of the macrophage inflammasome exacerbates inflammation in a zebrafish infection*
170 *model*
171 To confirm the results obtained with the sterile COVID-associated CSS model, we used
172 a bacterial infection model using *Salmonella enterica* serovar Typhimurium (ST) (Tyrkalska et
173 al., 2016). The results revealed that inflammasome inhibition in either neutrophils or
174 macrophages led to hiper susceptibility of the larvae to ST infection (Figures 2A-2B).
175 Moreover, macrophage inflammasome inhibition resulted in hyper inflammation at 24 hpi,
176 assayed as the transcript levels of *il1b* and *tnfa* (Figures 2C-2D). Although these results
177 confirmed the ones obtained with the S1WT-driven inflammation, we next examined
178 inflammation at shorter time points of the infectious process. Interestingly, at 6 hpi the
179 inhibition of macrophage inflammasome led to lower *il1b* and *tnfa* transcript levels, whereas at
180 12 hpi the opposite was observed (Figures 2E-2F). Collectively, these results revealed an
181 unappreciated role of the macrophage inflammasome in the resolution of inflammation. In sharp
182 contrast and confirming previous results with the S1WT-driven inflammation model, neutrophil
183 inflammasome inhibition led to decreased transcript levels of *il1b* and *tnfa* at 24 hpi (Figure
184 2G-H). As expected, inflammasome inhibition in both cell types decreased caspase-1 activity

levels in infected larvae (Figures 2I-2J). Notably, it was found again that inhibition of macrophage inflammasome resulted in a more robust decreased of caspase-1 activity than inhibition of neutrophil inflammasome.

We next examined immune cell recruitment and total number by injecting ST in the otic vesicle. On the one hand, while inhibition of macrophage inflammasome did not affect the recruitment of these cells (Figures 2K and S2A), the total number of macrophages increased in basal condition and upon ST infection at 1 hpi (Figures 2L and S2B). At later timepoints, however, macrophage inflammasome inhibition led to decreased macrophage number, probably reflecting their killing by ST (Figures 2L and S2B). On the other hand, neutrophil recruitment in the larvae with neutrophil inflammasome inhibition turned out to be potentiated as more neutrophils were recruited to the otic vesicle (Figures 2M and S2C). What is more, the total number of neutrophils increased upon inhibition of their inflammasome in basal condition and upon infection at all timepoints analyzed. However, neutrophil counts decreased in wild type larvae upon infection at 3 and 6 hpi (Figures 2N and S2D). These results suggest that ST promoted neutrophil killing through pyroptosis, while other cell death mechanisms should operate in macrophages.

Overactivation of neutrophil inflammasome leads to myeloid cell imbalance and attenuated inflammation

We next examined the impact of activation of either the neutrophil or the macrophage inflammasome. To do so, we generated the *Tg(lyz:Dendra-Asc)* which overexpressed Dendra-Asc driven by the neutrophil specific promoter *lyz* and additionally a green heart marker. We found that overactivation of neutrophil inflammasome resulted in increased larval resistance to bacterial infection (Figure 3A) and decreased inflammation at 24 hpi than their wild type siblings (Figures 3B-3C). These results were further confirmed using the Nfkb reporter line *Tg(nfkb:GFP)* where expression of Dendra-Asc in neutrophils robustly diminished ST-induced Nfkb reporter activity at 6 and 24 hpi (Figures 3D-3E and S3A-S3B). As expected, caspase-1 activity levels increased in *Tg(lyz:Dendra-Asc)* under basal and infection conditions, confirming the overactivation of the inflammasome (Figure 3F). Furthermore, larvae overexpressing Dendra-Asc in neutrophils exhibited reduced recruitment to ST at 1, 3, and 6 hpi compared to their control siblings (Figures 3G-3H and S3C-S3D), likely due to their lower neutrophil numbers in baseline and upon infection at all analyzed timepoints (Figures 3G-3H and S3C-S3D). As activation of the inflammasome may lead to pyroptosis, we used TUNEL assay combined with immunostaining of neutrophils with an anti-Mpx antibody. The results confirmed that neutrophil inflammasome overactivation led to higher number of TUNEL positive cells, lower number of neutrophils and higher percentage of TUNEL^{+} neutrophils than

221 their wild-type siblings (Figures 3I-3L and S3E). We then analyzed the number of macrophages
222 in *Tg(lyz:Dendra-Asc)* larvae and we observed higher number of macrophages than control
223 larvae, which explains their more robust recruitment to the bacterium (Figures 3M-3N and S3F-
224 S3G). Strikingly, macrophages of *Tg(lyz:Dendra-Asc)* larvae were resistant to ST killing
225 (Figures 3M-3N and S3F-S3G). Collectively, these results uncover a previously unrecognized
226 crosstalk between neutrophils and macrophages mediated by the inflammasome and further
227 suggest an anti-inflammatory role of macrophages in zebrafish larvae.

228 To further understand the effects of overactivation of the inflammasome in neutrophils
229 and the crosstalk between neutrophils and macrophages, we combined overactivation of
230 inflammasome in neutrophils using *Tg(lyz:Dendra-Asc)* together with inhibition of the
231 macrophage inflammasome expressing DN-Asc in macrophages. The results showed that
232 macrophage inflammasome inhibition abrogated the resistance of macrophages of
233 *Tg(lyz:Dendra-Asc)* to ST killing and the attenuated inflammatory response (Figures 3O-3R
234 and S3I-S3J). This suggests that crosstalk between neutrophil and macrophage inflammasomes
235 is crucial for regulating the inflammatory response, with the macrophage inflammasome
236 playing a previously unrecognized role in the resolution of inflammation.

237 Similar results were obtained with the COVID-19-associated CSS. Thus, the transcript
238 levels of *il1b* and *tnfa* were significantly lower in *Tg(lyz:Dendra-Asc)* larvae with than in their
239 wild-type siblings upon S1WT injection (Figures S4A-S4D). *Tg(lyz:Dendra-Asc)* larvae
240 showed higher caspase-1 activity than wild-type animals in both basal and upon S1WT injection
241 condition (Figures S4E-S4F). Finally, the immune cell behavior in larvae with overactivated
242 neutrophil inflammasome was like the one seen with bacterial infection: lower recruitment of
243 neutrophils to the site of the injection and lower number of neutrophils than in control larvae
244 (Figure S4G-S4I and S5A-S5B). However, although *Tg(lyz:Dendra-Asc)* larvae showed normal
245 recruitment of macrophages, they had much more macrophages in basal conditions and upon
246 S1WT injection (Figure S4J-S4L and S5C-S5D).

247

248 *Overactivation of the macrophage inflammasome leads to myeloid cell imbalance and*
249 *enhanced inflammation*

250 The phenotype observed following cell-specific activation of the inflammasome in
251 neutrophils prompted us to investigate the impact of macrophage inflammasome activation. To
252 this end, we microinjected the plasmid *mpeg1:Dendra-Asc* into one-cell stage embryos to
253 achieve transient expression of Dendra-Asc in macrophages. Attempts to generate a stable line
254 were unsuccessful, likely because overactivation of Dendra-Asc in macrophages may be lethal
255 to the fish. Unexpectedly, overactivation of macrophage inflammasome resulted in increased
256 larval susceptibility to ST infection (Figure 4A). Moreover, *mpeg1:Dendra-Asc* larvae showed

257 significantly higher inflammation in both basal and infected conditions than their wild-type
258 siblings, as assayed with the transcript levels of *il1b* and *tnfa* by RT-qPCR at 24 hpi (Figures
259 4B-4C). These results were further confirmed with the Nfkb reporter line *Tg(nfkb:eGFP)*,
260 where expression of Dendra-Asc in macrophages dramatically potentiated the levels of Nfkb
261 reporter activity in both uninfected and infected larvae (Figures 4D-4E and S6A-S6B). As
262 expected, overexpression of Dendra-Asc in macrophages led to increased caspase-1 activity
263 (Figure 4F).
264 We next analyzed neutrophil and macrophage behaviors in larvae with overactivation
265 of the macrophage inflammasome in response to infection. Stronger recruitment of neutrophils
266 to the bacteria in larvae expressing Dendra-Asc in macrophages than in control larvae was
267 found only at 1 hpi (Figures 4G-4H and S6C-S6D). This may be explained by the neutrophilia
268 found in *mpeg1:Dendra-Asc* uninfected and infected larvae and their killing by ST at 3 (Figures
269 4G-4H and S6C-S6D). In sharp contrast, the recruitment of macrophages in *mpeg1:Dendra-*
270 *Asc* larvae decreased in uninfected and infected conditions, probably because of the
271 monocytopenia observed in *mpeg1:Dendra-Asc* injected larvae (Figures 4I, 4J and S6E, S6F).
272 Therefore, cell-specific overactivation of the inflammasome led to pyroptotic cell death of both
273 neutrophils and macrophages.
274
275 *Extracellular ASC specks drive emergency myelopoiesis and hyperinflammation via*
276 *inflammasome activation*
277 These unexpected results, showing a crosstalk between neutrophil and macrophage
278 inflammasomes, together with the reported ability of extracellular ASC specks to propagate
279 inflammation (Baroja-Mazo et al., 2014; Franklin et al., 2014), led us to perform study the
280 impact of injecting human recombinant ASC protein in circulation of 2 dpf larvae. The results
281 showed increased number of neutrophils and macrophages at 1, 3, 6 and 24 hpi (Figures 5A-
282 5B and S7A, S7B). The injection itself, as well as the injection of BSA protein as a control, did
283 not cause any increase in the number of neutrophils or macrophages at any time point analyzed
284 (Figure 5A, 5B and S7A, S7B). Moreover, hASC injected larvae showed increased levels of
285 inflammation, namely higher transcript levels of *il1b* and *tnfa* at 3 and 24 hpi than the larvae
286 injected with BSA (Figure 5C). Curiously, inhibition of the canonical inflammasome with the
287 caspase-1 inhibitor VX-765 resulted in a dual effect: rapid attenuation and slow potentiation of
288 hASC-driven induction of *il1b* and *tnfa* (Figure 5C).
289 Finally, to confirm the role of phagocytosis of hASC specks by zebrafish myeloid cells,
290 wild-type larvae were treated with colchicine and then injected with hASC. The results showed
291 that colchicine was able to block hASC-induced neutrophilia, monocytosis and
292 hyperinflammation (Figures 5D-5F and S7C, S7D). Collectively, these results suggest that

hASC specks are taken up by neutrophils and macrophages, activating their inflammasomes to drive emergency myelopoiesis and inflammation. Furthermore, they further point out a dual role of the inflammasome in regulating inflammation.

Neutrophil to macrophage Asc speck transfer occurs in vivo

We next examined using the unique advantage of the zebrafish model for *in vivo* imaging whether Asc specks can be transferred from neutrophil to macrophage by using photoconvertible green to red fluorescent Dendra (Adam et al., 2009). We first examined Dendra-Asc in *Tg(lyz:Dendra-Asc)* with spinning disk confocal microscopy and found that it was expressed in neutrophils but with two different patterns: either uniformly distributed within the cell or forming Asc specks (Figure 6A). This suggests that overexpression of Dendra-Asc may induce Asc oligomerization without further stimulus, confirming our previous functional and caspase-1 activity results. We next photoconverted Dendra-Asc in the HBV of 2 dpf larvae and we imaged this area for green and red fluorescence 4.5 hours later, confirming photoconversion in several neutrophils (Figure 6B). This photoconversion approach was used in the COVID-19-associated CSS to image neutrophils present at the CHT at 4.5 hpi of S1WT-injected larvae. Green neutrophils with and without red Asc-specks were clearly visible (Figure 6C), suggesting that activated neutrophils wandered from HBV to CHT. Of note, while the total number of green neutrophils in the CHT was similar between control and S1WT-injected larvae, the S1WT-injected group showed a significantly higher number of neutrophils containing red fluorescent Asc-specks compared to their control siblings (Figure 6D).

This result prompted us to examine whether Asc-specks may be transferred from neutrophils to macrophages using *Tg(lyz:Dendra-Asc)*; *Tg(mfap4:mCherry-F)* line. Larvae of 2 dpf were injected with S1WT in the CHT to increase the formation of Dendra-Asc specks in neutrophils and Dendra-Asc speck transfer from neutrophils to macrophages was successfully observed at 4.5 hpi (Figure 6E). Thus, numerous red fluorescent macrophages were observed with green Dendra-Asc specks that originated in Dendra-Asc neutrophils (Figure 6E). Collectively, these results that Asc specks can be transferred from activated neutrophils to bystander neutrophils and from activated neutrophils to bystander macrophages.

Gsdme- and Ninj1-driven cell death mediate the crosstalk between neutrophils and macrophages

To study whether cell death is involved in the crosstalk between the inflammasome of neutrophils and macrophages, we inactivated the 2 paralogs of zebrafish Gasdermin E (Gsdmea and Gsdmeb), since GSDMD is only present in mammals (Angosto-Bazarra et al., 2023) and Gsdme operates downstream the inflammasome in zebrafish (Lozano-Gil et al., 2022;

329 Tyrkalska et al., 2023b). Gsmdea/b deficiency (edition efficiency of about 60%) fully rescued
330 the neutropenia of Tg(*lyz:Dendra-Asc*) larvae (Figures 7A and S7A) confirming that
331 overactivation of the neutrophil inflammasome resulted in Gsdmea/b-mediated pyroptosis of
332 these cells. Strikingly, the opposite effect was seen with macrophages, where Gsdmea/b
333 deficiency was able to reverse the monocytosis of Tg(*lyz:Dendra-Asc*) larvae to the levels of
334 the negative siblings (Figures 7B and S7B). In addition, Gsdmea/b deficiency was able to rescue
335 the low transcript levels of *il1b* and *tnfa* in larvae with overactivated neutrophil inflammasome
336 (Figure 7C, 7D). Similarly, depletion of Gdsmea/b was able to rescue both monocytopenia and
337 neutrophilia of larvae transiently expressing *mpeg1:Dendra-Asc* (Figures 7E, 7F and S7C,
338 S7D). In sharp contrast, the increased transcript levels of *il1b* and *tnfa* of larvae with
339 overactivated macrophage inflammasome was unaffected by Gsdmea/b deficiency (Figure 7G,
340 7H). Together, these results highlight the involvement of Gsdmea/b-mediated pyroptosis in the
341 crosstalk between neutrophils and macrophages and reveal that macrophage Gsdme acts as a
342 negative regulator of inflammation.

343 To confirm the above results, we incubated 1 dpf *Tg(lyz:Dendra-Asc)* larvae during 48
344 h with glycine, a plasma membrane rupture (PMR) inhibitor (Devant and Kagan, 2023;
345 Weinberg et al., 2016) and found that glycine was able to fully rescue the pyroptotic cell death
346 of neutrophils in *Tg(lyz:Dendra-Asc)* larvae and increased the total number of neutrophils in
347 their wild-type siblings (Figures 7I and S7E). Importantly, glycine also reversed the decreased
348 inflammation of infected *Tg(lyz:Dendra-Asc)* larvae (Figures 7J, 7K). Similarly, glycine
349 rescued the pyroptotic cell death of macrophages (Figures 7L and S7F) and decreased the
350 hyperinflammation induced by ST infection (Figures 7M, 7N). The same results were obtained
351 by knocking down Ninjurin-1 (Ninj1, KO efficiency of 80%) (Figure S8A-S8F), confirming
352 that Ninj1-driven PMR is required for the crosstalk between neutrophils and macrophages.

353 We further investigated the role played by Gsdme in the anti-inflammatory function of
354 macrophages by overexpressing catalytic-dead Caspa-C270A, which should behave as a DN
355 form. It was found that while hASC injection resulted in hyperinflammation in Gsdme-deficient
356 larvae, confirming the results with ST infection, expression of Caspa-C270A in neutrophils
357 fully abrogated the pro-inflammatory activity of hASC in both wild type and Gsdme-deficient
358 larvae (Figures S9A, S9B). In sharp contrast, the expression of DN-Caspa in macrophages led
359 to hyperinflammation independently of Gsdme (Figures S9C, S9D). Furthermore, although
360 Nlrp3 deficiency (KO efficiency of 75%) successfully abrogated infection-induced
361 inflammation and caspase-1 activity, it failed to mitigate the hyperinflammation and
362 exacerbated caspase-1 activity observed in Gsdme-deficient larvae (Figures S9E-S9G). These
363 findings underscore the pivotal role of Gsdme in the feedback inhibition of inflammasome
364 activity and highlight its importance in the regulation of inflammation by macrophages.

DISCUSSION

While the pro-inflammatory role of inflammasomes in regulating inflammation and immunity is well-established, their potential anti-inflammatory function remains largely unexplored. The name itself is associated with inflammatory processes leading to the release of cytokines and causing pyroptotic cell death (Martinon et al., 2002; Schroder and Tschopp, 2010). Inflammasomes are very potent inflammatory mediators that have always been studied as a set in the sense of the whole organism. Animal models available for inflammasome research are not adapted for the study of cell specific inflammasomes (Forn-Cuni et al., 2019; Garcia-Moreno et al., 2019; Guo and Ting, 2020). The lack of animal transparency and the scarcity of animal models specifically deficient for different inflammasome components make it difficult to study this area of research. Due to the growing importance of inflammasomes, their study has been extended to non-mammalian vertebrates such as zebrafish (Chang, 2023; Morimoto et al., 2021).

Both macrophages and neutrophils express the inflammasome components, which are ubiquitously present in the various cell types of the immune system. While macrophages and dendritic cells were initially credited with inflammasome activation and IL-1β production, neutrophils were traditionally regarded as recipients of pro-inflammatory cytokines (Tyrkalska et al., 2021). However, recent studies have demonstrated that NLRP3, NLRC4 and NLR12 inflammasomes can be activated by neutrophils during bacterial infections (Chen et al., 2014; Thomas and Schroder, 2013). The activation of well-studied macrophages NLRC4 inflammasome causes pyroptosis, while neutrophil inflammasome activation results in NETosis (Kayagaki et al., 2015). This distinction in neutrophils behavior may be explained by their ASC size and by the presence of multiple ASC specks per cell, whereas macrophages possess single individual specks (Boucher et al., 2018; Latz et al., 2013). What is more, in neutrophils, inflammasome activation leads to the robust production of IL-1β, while in macrophages, it triggers the release of IL-1β along with other cytokines, including IL-1α and IL18 (Bakele et al., 2014). Moreover, in macrophages, caspase-1 is more abundant and is primarily responsible for the production of IL-1β, whereas in neutrophils, IL-1β secretion is mostly mediated by serine proteases (Boucher et al., 2018). Additionally, recent study has revealed that neutrophils can also secrete IL-1β via an autophagy-dependent mechanism(Karmakar et al., 2020). Furthermore, in macrophages caspase-1 cleaves GSDMD and produces N-GSDMD p31 fragments, leading to the formation of plasma membrane pores, IL-1β release and pyroptosis. In contrast, in neutrophils although plasma membrane pores are formed by N-GSDMD p31 fragments, they do not induce pyroptosis (Karmakar et al., 2020). In turn, neutrophil caspase-4 and caspase-11 are activated via noncanonical inflammasome signaling, resulting in neutrophil

401 GSDMD-induced cell death called NETosis, and the induction of extrusion of host-protective
402 antimicrobial NETs (Chen et al., 2018; Sollberger et al., 2018; Tyrkalska et al., 2021). Likewise,
403 macrophage GBPs play a crucial role in inflammasome activation, IL-1β production and
404 pyroptosis induction. However, in neutrophils, GBPs only mediate prostaglandin biosynthesis
405 and release (Shenoy et al., 2012; Tyrkalska et al., 2016; Tyrkalska et al., 2021). Finally,
406 macrophages undergo pyroptosis, releasing ASC specks into the extracellular space. In contrast,
407 neutrophils release secretory vesicles containing inflammasome components, which serve to
408 amplify the inflammatory response (Baroja-Mazo et al., 2014; Franklin et al., 2014; Tyrkalska
409 et al., 2021).

410 Here, we show for the first time, using unique advantages of zebrafish model, opposed
411 roles of the in neutrophil and macrophage inflammasomes in *S*. Typhimurium infection
412 (Tyrkalska et al., 2016) and COVID-19-associated CRS (Tyrkalska et al., 2022) models, with
413 neutrophils being pro-inflammatory and macrophages being anti-inflammatory. To the best of
414 our knowledge this is the first study showing that the macrophage inflammasome plays an anti-
415 inflammatory role, suggesting that cell-specific inflammasome inhibition may be a more
416 effective therapeutic approach to treat intracellular bacterial infections, COVID-19-associated
417 CRS and even chronic inflammatory diseases. The zebrafish animal models developed here
418 with cell specific Asc loss- and gain-of-functions facilitate the study of cell specific
419 inflammasomes, not only neutrophils and macrophages but also other cell types where the
420 inflammasome play a relevant role.

421 One important observation from our study is that DN Asc was able to block
422 inflammasome activation in both neutrophils and macrophages leading to hypersusceptibility
423 to *S*. Typhimurium, confirming previous results obtaining by knocking-down Asc in all cells of
424 the zebrafish larvae (Tyrkalska et al., 2016). Furthermore, these studies also revealed that *S*.
425 Typhimurium killed zebrafish neutrophils by pyroptosis, whereas macrophages were killed by
426 another programmed cell death mechanism. Although the contribution of macrophages and
427 neutrophils inflammasome in intracellular bacterial clearance and the relevance of pyroptosis
428 is complex, the crosstalk between these myeloid cells has already been appreciated. For
429 example, in vivo mouse models, NLRC4 inflammasome activation induces pyroptotic cell
430 death in macrophages, resulting in the release of intracellular bacteria, including *S*.
431 Typhimurium, *Legionella pneumophila* and *Burkholderia thailandensis*, which are then
432 exposed to uptake and killing by reactive oxygen species in neutrophils (Miao et al., 2010).
433 Furthermore, neutrophils are also the main contributors to IL-1β release in mice (Chen et al.,
434 2014) and eicosanoids in zebrafish (Tyrkalska et al., 2016) during *S*. Typhimurium infection,
435 since they are highly resistant to pyroptosis in both species.

436 Our study has also revealed a previously unappreciated crosstalk between neutrophil
437 and macrophage inflammasomes. Thus, overactivation of neutrophil inflammasome by
438 expressing Dendra-Asc promoted their Gsdme-mediated pyroptotic cell death, although
439 apoptosis and necroptosis were also involved, and an unexpected increase of the number of
440 macrophages in basal conditions. Both effects were further altered in both inflammation
441 models, leading to high bacterial resistance and reduced inflammation. More importantly,
442 overactivation of the neutrophil inflammasome rendered macrophages resistant to *S.*
443 Typhimurium killing, whereas inhibition of macrophage inflammasome by specifically
444 expressing DN Asc was unable to protect these cells from bacterial killing. These results agree
445 with previous observations obtained overexpressing different inflammasome components in
446 whole larvae (Tyrkalska et al., 2016). Conversely, overactivation of macrophage inflammasome
447 resulted in Gsdme-mediated pyroptosis of macrophages and increased number of neutrophils,
448 leading to larval hypersusceptibility to the infection and exacerbated inflammation. Notably,
449 this crosstalk between neutrophils and macrophages is strictly dependent on Gsdme and cell
450 death, since Gsdme deficiency, and genetic and pharmacological (glycine administration)
451 inhibition of Ninj1, which block PMR (Devant and Kagan, 2023; Weinberg et al., 2016),
452 reversed cell number alterations. Both cell types are known to undergo pyroptosis, however this
453 process has been barely related to inflammation resolution (Bergsbaken and Cookson, 2007;
454 Brennan and Cookson, 2000; Dubyak et al., 2023; Fink and Cookson, 2006, 2019). Most of the
455 studies have already demonstrated the GSDMD, functional homolog of zebrafish Gsdme,
456 proinflammatory properties and an important role in host response to bacterial infection
457 (Aglietti et al., 2016; Chen et al., 2016). Using cell specific expression systems, we have
458 demonstrated for the first time Gsdme-dependent anti-inflammatory properties of macrophages.
459 What is interesting, macrophages show higher expression of Gsdmea comparing with
460 neutrophils, which may be the reason for the anti-inflammatory differences between those two
461 innate immune cells.

462 Since our results suggest a crosstalk between neutrophil and macrophage inflammasome
463 and Asc specks have been found in the serum of patients with chronic inflammatory diseases
464 and can be taken up by macrophages and activate their inflammasome (Baroja-Mazo et al.,
465 2014; Franklin et al., 2014), we hypothesized that released Asc specks contribute to the
466 spreading of inflammation. Therefore, we generated Tg(*lyz:Dendra-Asc*) line to track Asc
467 specks in vivo using photoconvertible Dendra fluorescent green-to-red protein (Lopez et al.,
468 2017). Taking advantage of this line, we were able to visualize for the first time Asc speck
469 formation, spreading and transfer in vivo from S1WT-activated neutrophils to bystander
470 neutrophils and macrophages, which further support a role for ASC speck release in the
471 spreading of inflammation in chronic inflammatory and infectious diseases and their roles in

472 the observed crosstalk between neutrophils and macrophages. We also observed that neutrophils
473 expressing Dendra-Asc showed two different phenotypes: uniform distribution of Asc within
474 the cell and cells with already formed Asc specks, confirming that overexpression of Asc alone
475 is able to initiate Asc speck formation and inflammasome activation without further stimuli
476 (Dick et al., 2016). Furthermore, the number of Asc-speck positive neutrophils increased in
477 COVID-19-associated CRS model, promoting Asc specks released and uptake by bystander
478 macrophages. Although additional experiments are needed to confirm that the transfer of Asc
479 specks between neutrophils and macrophages regulates the inflammatory response, the
480 increased inflammation and neutrophilia/monocytosis observed upon injection of recombinant
481 hASC strongly support this notion.

482 The most important discovery of our study is the novel role of macrophage
483 inflammasome in the resolution of inflammation. Although it is well known the crucial role
484 played by macrophages in the resolution of inflammation and their plasticity to polarize to
485 different phenotypes, including anti-inflammatory M2 macrophages, as they scan for danger
486 signals and maintain tissue homeostasis, the role of their inflammasome in this process is
487 unknown (Das et al., 2015; Mantovani et al., 2013; Patel et al., 2017). Furthermore, it is clear
488 that neutrophil-macrophage cooperation and direct interactions between them impact on the
489 final outcome of their functions (Bouchery and Harris, 2019; Chen et al., 2024). Using zebrafish
490 model, we uncovered another piece of complexity to the interactions of these cells: neutrophil
491 pyroptosis results in the releases of Asc specks into intracellular space, which can be uptaken
492 by bystander macrophages promoting inflammasome activation, Gsdme processing, Ninj1-
493 mediated PMR and enhanced anti-inflammatory properties. The anti-inflammatory properties
494 of Gsdme are not unexpected, since mouse GSDMD has been found to play both pro- and anti-
495 inflammatory roles (Kambara et al., 2018), and directly inhibits CASP1 activity (Hu et al.,
496 2022). In fact, the tetrapeptide of its N-terminal fragment essential for the inhibition of CASP1
497 is relatively well conserved in zebrafish Gsdmea and Gsdmeb (RFWK in mouse and WFWK
498 in human GDSDMD, and WFWQ in zebrafish Gsdmea/b). It remains to be elucidated why
499 macrophage Gsdme, but not neutrophil Gsdme, can play this anti-inflammatory role.

500 In summary, we present a unique model to study the impact of cell-specific
501 inflammasomes in intracellular bacterial infection and COVID-19-associated CRS. Our
502 findings demonstrate that neutrophil and macrophage inflammasomes play opposing roles in
503 regulating inflammation, highlighting the importance of Gsdme in resolving inflammation, akin
504 to mammalian GSDMD. Furthermore, we provide novel evidence of the transfer of Asc specks
505 from activated neutrophils to bystander neutrophils and macrophages in vivo. Understanding
506 the intricacies of this process opens new horizons for developing therapeutic targets to treat
507 inflammasome-dependent infectious and chronic inflammatory diseases.

508

509 **MATERIALS AND METHODS**

510 *Animals*

511 Zebrafish (*Danio rerio* H.) were obtained from the Zebrafish International Resource
512 Center and mated, staged, raised and processed as described (Westerfield, 2000). The lines
513 Tg(*lyz:dsRED*)^{nz50} (Hall et al., 2007), Tg(*mpx:eGFP*)^{i114} (Renshaw et al., 2006),
514 Tg(*mfap4:mCherry-F*)^{ump6} (Phan et al., 2018), Tg(*mfap4:tomato*)^{xt12} (Walton et al., 2015),
515 Tg(*mpeg1:mCherry/tnfa:eGFP-F*)^{ump5} (Nguyen-Chi et al., 2015), Tg(*mpeg1:GAL4*)^{gl25} (Ellett
516 et al., 2011), Tg(*mpx:Gal4.VP16*)^{i222} (Davison et al., 2007), Tg(*NFkB-RE:eGFP*)^{sh235} referred
517 to as nfkb:eGFP (Kanther et al., 2011), Tg(*UAS:ascΔCARD-GFP*)^{ums4} (Tyrkalska et al., 2019),
518 Tg(*UAS:nfsB-mCherry*)^{c264} (Davison et al., 2007), and casper (*mitfaw2/w2; mpv17a9/a9*)
519 (White et al., 2008) were previously described. The experiments performed comply with the
520 Guidelines of the European Union Council (Directive 2010/63/EU) and the Spanish RD
521 53/2013. The experiments and procedures were performed approved by the Bioethical
522 Committees of the University of Murcia (approval number #395/2017). All experiments were
523 performed with embryos/larvae less than 5 dpf.

524

525 *DNA Construct and Generation of Transgenics*

526 The *lyz:Dendra-Asc*, *mpeg1:Dendra-Asc*, *mfap4:dn-Asc* and *uas:dn-caspa* constructs were
527 generated by MultiSite Gateway assemblies using LR Clonase II Plus (Life Technologies)
528 according to standard protocols and using Tol2kit vectors described previously (Kwan et al.,
529 2007). The expression construct of Gcsfa (Liongue et al., 2009) was previously described. The
530 expression construct of NT-Gsdmea, CT-Gsdmea, full-length wild-type and D256A mutant
531 Gsdmea were synthetized in GeneScript.

532 Tg(*lyz:Dendra-Asc*) and Tg(*uas:DN-caspa*) were generated by microinjecting 0.5–1 nl
533 into the yolk sac of one-cell-stage embryos a solution containing 50 ng/µl *lyz:Dendra-Asc*
534 construct, respectively, and 150 ng/µl Tol2 RNA in microinjection buffer (× 0.5 Tango buffer
535 and 0.05% phenol red solution) using a microinjector (Narishige).

536

537 *CRISPR and RNA injection in zebrafish*

538 crRNA for zebrafish gsdmea, gsdmeb and negative control crRNA (Catalog #1072544),
539 and tracrRNA were purchased from IDT and resuspended in Nuclease-Free Duplex Buffer to
540 100 µM. 1µl of each was mixed and incubated for 5 min at 95 0C for duplexing. After removing
541 from the heat and cooling to room temperature, 1.43 µl of Nuclease-Free Duplex Buffer was
542 added to the duplex, giving a final concentration of 1000 ng/µl. Finally, the injection mix was
543 prepared by mixing 1 µl of duplex, 2.55 µl of Nuclease-Free Duplex Buffer, 0.25 µl Cas9

544 Nuclease V3 (IDT, #1081058) and 0.25 µl of phenol red, giving final concentrations of 250
545 ng/µl of gRNA duplex and 500 ng/µl of Cas9. The prepared mix was microinjected into the
546 yolk of one- to eight-cell-stage embryos using a microinjector (Narishige) (0.5–1 nl per
547 embryo). The same amounts of gRNA were used in all the experimental groups. The efficiency
548 of gRNA was checked by amplifying the target sequence with a specific pair of primers (Table
549 S1) and the TIDE webtool (https://tide.nki.nl/).
550 In vitro-transcribed RNA was obtained following manufacturer's instructions
551 (mMESSAGE mMACHINE kit, Ambion). RNA was mixed in microinjection buffer and
552 microinjected into the yolk of one-cell-stage embryos using a microinjector (Narishige; 0.5–
553 1 nl per embryo). The same amount of RNA was used for all the experimental groups.
554
555 *Chemical treatments*
556 In some experiments, 1 dpf embryos were manually dechorionated and treated for 1 to
557 3 dpf at 28°C by bath immersion with Metronidazole (Mtz, 5 mM, Sigma-Aldrich) in egg water
558 supplemented with 1% DMSO. In some experiments, 24 hpf embryos were treated with 0.3%
559 N-Phenylthiourea (PTU, Sigma-Aldrich) to inhibit melanogenesis.
560 For image acquisition and cell count experiments, 1-day postfertilization (dpf) embryos
561 were manually dechorionated and treated until 48 hpf by bath immersion with Glycine (Sigma-
562 Aldrich, #G7126) at final concentration of 1 or 50 mM diluted in egg water, Z-DEVD-FMK
563 (MedChemExpress (MCE), #HY-12466) at final concentration of 50 µM diluted in egg water,
564 VX-765 (Belnacasan, Selleckchem) at final concentration of 100 µM diluted in egg water and
565 Necrostatin-2 (MedChemExpress (MCE), #HY-14622A) at final concentration 10 µM diluted
566 in egg water. For gene expression experiments, 2 dpf were anesthetized in embryo medium
567 with 0.16 mg/mL tricaine and 10 bacteria/zebrafish were injected into the yolk sac, glycine
568 treatment was refreshed and maintained until 3 dpf (24 hpi) when larvae were collected for
569 further analysis.
570 Larvae of 2 dpf were treated with 1 mg/ml Colchicine (MedChemExpress, #HY-16569)
571 for 30 min before hASC injection and remained until 1 hpi until *in vivo* imaging was initiated.
572
573 *Recombinant protein injection*
574 Recombinant His-tagged Spike S1 wild-type produced in baculovirus-insect cells and
575 with <1.0 EU per µg protein as determined by the LAL method (#40591-V08B1, Sino
576 Biological) at a concentration of 0.25 mg/ml supplemented with phenol red were injected into
577 the hindbrain ventricle (1 nl) of 48 hpf zebrafish larvae (Tyrkalska et al., 2022; Tyrkalska et al.,
578 2023a).

579 Recombinant hASC (#CSB-EP890936HU, Cusabio) was resuspended in sterile water
580 at the concentration of 1 mg/ml. Larvae of 2 dpf were anesthetized in embryo medium with
581 0.16 mg/mL tricaine and hASC (1 mg/ml), BSA (1 mg/ml) or sterile water was injected into the
582 pericardium where it is directly drained to blood. The larvae were allowed to recover in egg
583 water at 29°C, and monitored for clinical signs of inflammation.
584
585 *Infection assays*
586 For infection experiments, ST 12023 (WT) was used. Overnight cultures in Luria-
587 Bertani (LB) broth were diluted 1/5 in LB with 0.3 M NaCl, incubated at 37 °C until 1.5 optical
588 density at 600 nm was reached, and finally diluted in sterile PBS. Larvae of 2 dpf were
589 anaesthetized in embryo medium with 0.16 mg ml−1 tricaine and 10 bacteria (yolk sac) or 100
590 (otic vesicle) per larvae were microinjected. Larvae were allowed to recover in egg water at
591 28–29 °C and monitored for clinical signs of disease or mortality over 5 days. At least three
592 independent experiments were performed with a total number of 200–350 larvae per treatment.
593
594 *Analysis of gene expression*
595 Total RNA was extracted from whole larvae or head/tail larvae with TRIzol reagent
596 (Invitrogen) following the manufacturer's instructions and treated with DNase I, amplification
597 grade (1 U/mg RNA: Invitrogen). SuperScript IV RNase H Reverse Transcriptase (Invitrogen)
598 was used to synthesize first-strand cDNA with random primer from 1µg of total RNA at 50 ^{0}C
599 for 50 min. Real-time PCR was performed with an ABIPRISM 7500 instrument (Applied
600 Biosystems) using SYBR Green PCR Core Reagents (Applied Biosystems). Reaction mixtures
601 were incubated for 10 min at 95 ^{0}C, followed by 40 cycles of 15 s at 95 ^{0}C, 1 min at 60 ^{0}C, and
602 finally 15 s at 95 ^{0}C, 1 min 60 ^{0}C, and 15 s at 95 ^{0}C. For each mRNA, gene expression was
603 normalized to the ribosomal protein S11 gene (*rps11*) content in each sample, using the Pfaffl
604 method (Pfaffl, 2001). The primers used are shown in Table S2. In all cases, each PCR was
605 performed with triplicate samples and repeated at least with two independent samples.
606
607 *Caspase-1 activity assays*
608 The caspase-1 activity was determined with the fluorometric substrate Z-YVAD 7-
609 Amido-4-trifluoromethylcoumarin (Z-YVAD-AFC, caspase-1 substrate VI, Calbiochem), as
610 described previously (Tyrkalska et al., 2016; Tyrkalska et al., 2019). In brief, 25–35 whole
611 larvae or 45 heads/tails were lysed in hypotonic cell lysis buffer (25 mM 4-(2-hydroxyethyl)
612 piperazine-1-ethanesulfonic acid, 5 mM ethylene glycol-bis(2-aminoethylether)-N,N,N′,N′-
613 tetraacetic acid, 5 mM dithiothreitol, 1:20 protease inhibitor cocktail (Sigma-Aldrich), pH 7.5)
614 on ice for 10 min. For each reaction, 100 µg protein were incubated for 90 min at room

temperature with 50 mM YVAD-AFC and 50 µl of reaction buffer (0.2% 3-[(3-cholamidopropyl)dimethylammonio]-1-propanesulfonate (CHAPS), 0.2 M 4-(2-hydroxyethyl) piperazine-1-ethanesulfonicacid, 20% sucrose, 29 mM dithiothreitol, pH 7.5). After incubation, the fluorescence of the AFC released from the Z-YVAD-AFC substrate was measured with a FLUOstart spectofluorometer (BGM, LabTechnologies) at an excitation wavelength of 405 nm and an emission wavelength of 492 nm. A representative caspase-1 activity graph out of three repeats is shown in figures.

Imaging of zebrafish larvae

To study immune cell recruitment to the injection site and Nfkb activation, 2 dpf *Tg(mpx:eGFP)*, *Tg(mfap4:tomato)* or *Tg(nfkb:egfp)* larvae were anaesthetized in embryo medium with 0.16 mg/ml tricaine. Images of the hindbrain, head or the whole-body area were taken 1, 3, 6, 12 and 24 h post-injection (hpi) using a Leica MZ16F fluorescence stereomicroscope. The number of neutrophils or macrophages was determined by counting visually and the fluorescence intensity was obtained and analyzed with ImageJ (FIJI) software (Schindelin et al., 2012). In all experiments, images were pooled from at least 3 independent experiments performed by two people and using blinded samples.

For laser confocal microscopy imaging, larvae were anesthetized in 200 µg/ml tricaine, mounted on 35 mm glass-bottom dishes (WillCo-dish), immobilized in 1% low-melting-point agarose and covered with 2 ml egg water supplemented with 160 µg/ml tricaine. Epi-fluorescent microscopy was performed using a MVX10 Olympus MacroView microscope (MVPLAPO 1X objective and XC50 camera). Confocal microscopy was performed on ANDOR CSU-W1 confocal spinning disk on an inverted NIKON microscope (Ti Eclipse) with ANDOR Neo sCMOS camera (20x air/NA 0.75 objective); laser 488 nm for GFP and 561 nm for mCherry. Image stacks for time-lapse movies were acquired at 28°C. The 4D files generated from time-lapse acquisitions were analyzed using Image J, adjusting brightness and contrast for maximal visibility.

For photoconversion of Dendra protein, Tg(lyz:Dendra-Asc) embryos were raised to 2 dpf in the dark, and S1WT-injected larvae in the Hindbrain Ventricle (HBV), as described above, were mounted in 1% low-melting point agarose. A 405-nm Laser Cube 405-50C on a confocal TCS SP5 inverted microscope with HCXPL APO 40x/1.25-0.75 oil objective (Leica) was used to photoconvert the Dendra-labelled cells using 10% laser power (optimized before the experiments). HBVs were imaged before and after the photoconversion in the green (488 nm) and red (561 nm) channels.

TUNEL assay and immunohistochemistry staining

The number of apoptotic cells in 3 dpf larvae was assessed by TUNEL assay. The larvae were fixed with 4% paraformaldehyde for 2 hours and dehydrated with methanol at -20°C. After gradual rehydration, the embryos were treated with 100% acetone at -20ºC for 10 min and rinsed 3 times for 10 min with PBT. Embryos were permeabilized with a solution containing 0.1% Triton X-100 and 0.1% sodium citrate in PBS for 30 minutes at RT and rinsed 2 times for 5 min with PBT. They were then washed 5 times with PBST for 5 minutes each and blocked in 10% calf serum, 1% DMSO, 0.1% Tween-20 for 1 h to initiate whole body immunohistochemistry staining (WIHC).

To label neutrophils, larvae were incubated with anti-Mpx antibody overnight at 4ºC (Genetex #GTX128379, 1:150), rinsed 5 times for 5 min with PBST, incubated with a secondary antibody (Invitrogen #A21207, 1:250) for 1 hour and, finally, rinsed 3 times for 5 min with PBST and stored in 70% glycerol in PBS until image acquisition. Images were acquired in a Leica MZ16F fluorescence stereo microscope.

Neutral Red Staining

Neutral red stains zebrafish macrophages granules and the procedure was performed as originally reported (Herbomel et al., 2001). Briefly, macrophage staining was performed on live 3dpf larvae and was obtained by the incubation of the embryos in 2.5 g/ml of neutral red solution from Sigma-Aldrich (in embryo medium) at 25–30°C in the dark for 5-8 h. The larvae were anesthetized in 0.16 mg ml-1 tricaine and imaged using a Leica MZ16F fluorescence stereo microscope.

Statistical analysis

Statistical analysis was performed using Prism 8.0 (GraphPad Software, CA, USA). No calculation was performed to predetermine sample size; experiments were repeated three times to ensure robustness. Embryos were randomly allocated to each experimental condition and analyzed in blind samples. No data were excluded from the analysis. Data are shown as mean ± s.e.m. and were analyzed by analysis of variance and a Tukey multiple range test to determine differences between groups. The differences between the two samples were analyzed by the two-sided Student's t-test. The data met normal distribution assumption when required and showed similar variances. A log-rank test was used to calculate the statistical differences in the survival of the different experimental groups. A p-value of <0.05 was considered statistically significant.

CONFLICT OF INTEREST

The authors declare no conflict of interest.

ACKNOWLEDGMENTS

We warmly thank I. Fuentes, P. Martínez, M. Rodenas and ME Rubio for their excellent technical assistance. We also thank Profs. S.A. Renshaw, P. Crosier, A.H. Meijer, D. Tobin and L.I. Zon for the zebrafish lines.

FINANCIAL DISCLOSURE

This work was supported by research grant by Instituto de Salud Carlos III (ISCIII) through the project "CP23/00049" and Spanish Ministry of Science and Innovation (Juan de la Cierva-Incorporacion postdoctoral contract) to SDT, Fundación Séneca, Agencia de Ciencia y Tecnología de la Región de Murcia (grant 21887/PI/22 to VM and SDT), MCIN/AEI/10.13039/501100011033 (research grants 2020-113660RB-I00 to VM, the European Union's Horizon 2020 research and innovation program under the Marie Skłodowska-Curie (grant agreement No.955576 – INFLANET) and the Spanish Ministry of Universities (PhD fellowship to JML-G). The funders had no role in the study design, data collection and analysis, decision to publish, or preparation of the manuscript.

AUTHOR CONTRIBUTIONS

SDT and VM conceived the study; SDT, AP, JMLG, MENC and GL performed the research; SDT, AP, JMLG, MENC, GL and VM analyzed the data; and SDT and VM wrote the manuscript with minor contributions from other authors.

BIBLIOGRAPHY

Adam, V., Nienhaus, K., Bourgeois, D., and Nienhaus, G.U. (2009). Structural basis of enhanced photoconversion yield in green fluorescent protein-like protein Dendra2. Biochemistry *48*, 4905-4915.

Aglietti, R.A., Estevez, A., Gupta, A., Ramirez, M.G., Liu, P.S., Kayagaki, N., Ciferri, C., Dixit, V.M., and Dueber, E.C. (2016). GsdmD p30 elicited by caspase-11 during pyroptosis forms pores in membranes. Proc Natl Acad Sci U S A *113*, 7858-7863.

Angosto-Bazarra, D., Guijarro, A., and Pelegrin, P. (2023). Evolution of the gasdermin family and pyroptosis. Dev Comp Immunol *149*, 105060.

Bakele, M., Joos, M., Burdi, S., Allgaier, N., Pöschel, S., Fehrenbacher, B., Schaller, M., Marcos, V., Kümmerle-Deschner, J., Rieber, N., *et al.* (2014). Localization and functionality of the inflammasome in neutrophils. The Journal of biological chemistry *289*, 5320-5329.

Baroja-Mazo, A., Martin-Sanchez, F., Gomez, A.I., Martinez, C.M., Amores-Iniesta, J., Compan, V., Barbera-Cremades, M., Yague, J., Ruiz-Ortiz, E., Anton, J., *et al.* (2014). The NLRP3 inflammasome is released as a particulate danger signal that amplifies the inflammatory response. Nat Immunol *15*, 738-748.

Bergsbaken, T., and Cookson, B.T. (2007). Macrophage activation redirects yersinia-infected host cell death from apoptosis to caspase-1-dependent pyroptosis. PLoS Pathog *3*, e161.

Boucher, D., Monteleone, M., Coll, R.C., Chen, K.W., Ross, C.M., Teo, J.L., Gomez, G.A., Holley, C.L., Bierschenk, D., Stacey, K.J., *et al.* (2018). Caspase-1 self-cleavage is an intrinsic mechanism to terminate inflammasome activity. J Exp Med *215*, 827-840.

Bouchery, T., and Harris, N. (2019). Neutrophil-macrophage cooperation and its impact on tissue repair. Immunol Cell Biol *97*, 289-298.

Brennan, M.A., and Cookson, B.T. (2000). Salmonella induces macrophage death by caspase-1-dependent necrosis. Mol Microbiol *38*, 31-40.

Cai, X., Chen, J., Xu, H., Liu, S., Jiang, Q.X., Halfmann, R., and Chen, Z.J. (2014). Prion-like polymerization underlies signal transduction in antiviral immune defense and inflammasome activation. Cell *156*, 1207-1222.

Chang, M.X. (2023). Emerging mechanisms and functions of inflammasome complexes in teleost fish. Front Immunol *14*, 1065181.

Chen, K.W., Gross, C.J., Sotomayor, F.V., Stacey, K.J., Tschopp, J., Sweet, M.J., and Schroder, K. (2014). The neutrophil NLRC4 inflammasome selectively promotes IL-1beta maturation without pyroptosis during acute Salmonella challenge. Cell Rep *8*, 570-582.

Chen, K.W., Monteleone, M., Boucher, D., Sollberger, G., Ramnath, D., Condon, N.D., von Pein, J.B., Broz, P., Sweet, M.J., and Schroder, K. (2018). Noncanonical inflammasome signaling elicits gasdermin D-dependent neutrophil extracellular traps. Sci Immunol *3*.

Chen, X., He, W.T., Hu, L., Li, J., Fang, Y., Wang, X., Xu, X., Wang, Z., Huang, K., and Han, J. (2016). Pyroptosis is driven by non-selective gasdermin-D pore and its morphology is different from MLKL channel-mediated necroptosis. Cell Res *26*, 1007-1020.

Chen, Y., Yang, Y., Lu, J., Chen, H., Shi, Z., Wang, X., Xu, N., Xu, X., and Wang, S. (2024). Neutrophil and macrophage crosstalk might be a potential target for liver regeneration. FEBS Open Bio.

Das, A., Sinha, M., Datta, S., Abas, M., Chaffee, S., Sen, C.K., and Roy, S. (2015). Monocyte and macrophage plasticity in tissue repair and regeneration. Am J Pathol *185*, 2596-2606.

Davison, J.M., Akitake, C.M., Goll, M.G., Rhee, J.M., Gosse, N., Baier, H., Halpern, M.E., Leach, S.D., and Parsons, M.J. (2007). Transactivation from Gal4-VP16 transgenic insertions for tissue-specific cell labeling and ablation in zebrafish. Dev Biol *304*, 811-824.

Devant, P., and Kagan, J.C. (2023). Molecular mechanisms of gasdermin D pore-forming activity. Nat Immunol *24*, 1064-1075.

Dick, M.S., Sborgi, L., Ruhl, S., Hiller, S., and Broz, P. (2016). ASC filament formation serves as a signal amplification mechanism for inflammasomes. Nat Commun *7*, 11929.

Dubyak, G.R., Miller, B.A., and Pearlman, E. (2023). Pyroptosis in neutrophils: Multimodal integration of inflammasome and regulated cell death signaling pathways. Immunol Rev *314*, 229-249.

Ellett, F., Pase, L., Hayman, J.W., Andrianopoulos, A., and Lieschke, G.J. (2011). mpeg1 promoter transgenes direct macrophage-lineage expression in zebrafish. Blood *117*, e49-56.

Fink, S.L., and Cookson, B.T. (2006). Caspase-1-dependent pore formation during pyroptosis leads to osmotic lysis of infected host macrophages. Cell Microbiol *8*, 1812-1825.

Fink, S.L., and Cookson, B.T. (2019). Pillars Article: Caspase-1-dependent pore formation during pyroptosis leads to osmotic lysis of infected host macrophages. Cell Microbiol. 2006. 8: 1812-1825. J Immunol *202*, 1913-1926.

Forn-Cuni, G., Meijer, A.H., and Varela, M. (2019). Zebrafish in Inflammasome Research. Cells *8*.

Forrest, O.A., Dobosh, B., Ingersoll, S.A., Rao, S., Rojas, A., Laval, J., Alvarez, J.A., Brown, M.R., Tangpricha, V., and Tirouvanziam, R. (2022). Neutrophil-derived extracellular vesicles promote feed-forward inflammasome signaling in cystic fibrosis airways. J Leukoc Biol *112*, 707-716.

Franklin, B.S., Bossaller, L., De Nardo, D., Ratter, J.M., Stutz, A., Engels, G., Brenker, C., Nordhoff, M., Mirandola, S.R., Al-Amoudi, A., *et al.* (2014). The adaptor ASC has extracellular and 'prionoid' activities that propagate inflammation. Nat Immunol *15*, 727-737.

Fu, J., Schroder, K., and Wu, H. (2024). Mechanistic insights from inflammasome structures. Nat Rev Immunol.

Garcia-Moreno, D., Tyrkalska, S.D., Valera-Perez, A., Gomez-Abenza, E., Perez-Oliva, A.B., and Mulero, V. (2019). The zebrafish: A research model to understand the evolution of vertebrate immunity. Fish Shellfish Immunol *90*, 215-222.

Guo, H., and Ting, J.P. (2020). Inflammasome Assays In Vitro and in Mouse Models. Curr Protoc Immunol *131*, e107.

Hall, C., Flores, M.V., Storm, T., Crosier, K., and Crosier, P. (2007). The zebrafish lysozyme C promoter drives myeloid-specific expression in transgenic fish. BMC Dev Biol *7*, 42.

Herbomel, P., Thisse, B., and Thisse, C. (2001). Zebrafish early macrophages colonize cephalic mesenchyme and developing brain, retina, and epidermis through a M-CSF receptor-dependent invasive process. Dev Biol *238*, 274-288.

Hickey, M.J., and Kubes, P. (2009). Intravascular immunity: the host-pathogen encounter in blood vessels. Nature reviews Immunology *9*, 364-375.

Hu, Y., Jiang, Y., Li, S., Ma, X., Chen, M., Yang, R., Wen, S., Moynagh, P.N., Wang, B., Hu, G.*, et al.* (2022). The Gasdermin D N-terminal fragment acts as a negative feedback system to inhibit inflammasome-mediated activation of Caspase-1/11. Proc Natl Acad Sci U S A *119*, e2210809119.

Kambara, H., Liu, F., Zhang, X., Liu, P., Bajrami, B., Teng, Y., Zhao, L., Zhou, S., Yu, H., Zhou, W.*, et al.* (2018). Gasdermin D Exerts Anti-inflammatory Effects by Promoting Neutrophil Death. Cell Rep *22*, 2924-2936.

Kanther, M., Sun, X., Muhlbauer, M., Mackey, L.C., Flynn, E.J., 3rd, Bagnat, M., Jobin, C., and Rawls, J.F. (2011). Microbial colonization induces dynamic temporal and spatial patterns of NF-kappaB activation in the zebrafish digestive tract. Gastroenterology *141*, 197-207.

Karmakar, M., Minns, M., Greenberg, E.N., Diaz-Aponte, J., Pestonjamasp, K., Johnson, J.L., Rathkey, J.K., Abbott, D.W., Wang, K., Shao, F.*, et al.* (2020). N-GSDMD trafficking to neutrophil organelles facilitates IL-1beta release independently of plasma membrane pores and pyroptosis. Nat Commun *11*, 2212.

Kayagaki, N., Stowe, I.B., Lee, B.L., O'Rourke, K., Anderson, K., Warming, S., Cuellar, T., Haley, B., Roose-Girma, M., Phung, Q.T.*, et al.* (2015). Caspase-11 cleaves gasdermin D for non-canonical inflammasome signalling. Nature *526*, 666-671.

Kolaczkowska, E., and Kubes, P. (2013). Neutrophil recruitment and function in health and inflammation. Nature reviews Immunology *13*, 159-175.

Kwan, K.M., Fujimoto, E., Grabher, C., Mangum, B.D., Hardy, M.E., Campbell, D.S., Parant, J.M., Yost, H.J., Kanki, J.P., and Chien, C.B. (2007). The Tol2kit: a multisite gateway-based construction kit for Tol2 transposon transgenesis constructs. Dev Dyn *236*, 3088-3099.

Latz, E., Xiao, T.S., and Stutz, A. (2013). Activation and regulation of the inflammasomes. Nat Rev Immunol *13*, 397-411.

Lendeckel, U., Venz, S., and Wolke, C. (2022). Macrophages: shapes and functions. ChemTexts *8*, 12.

Liongue, C., Hall, C.J., O'Connell, B.A., Crosier, P., and Ward, A.C. (2009). Zebrafish granulocyte colony-stimulating factor receptor signaling promotes myelopoiesis and myeloid cell migration. Blood *113*, 2535-2546.

Lopez, A., Lee, S.E., Wojta, K., Ramos, E.M., Klein, E., Chen, J., Boxer, A.L., Gorno-Tempini, M.L., Geschwind, D.H., Schlotawa, L.*, et al.* (2017). A152T tau allele causes neurodegeneration that can be ameliorated in a zebrafish model by autophagy induction. Brain *140*, 1128-1146.

Lozano-Gil, J.M., Rodriguez-Ruiz, L., Tyrkalska, S.D., Garcia-Moreno, D., Perez-Oliva, A.B., and Mulero, V. (2022). Gasdermin E mediates pyroptotic cell death of neutrophils and macrophages in a zebrafish model of chronic skin inflammation. Dev Comp Immunol, 104404.

Lu, A., Magupalli, V.G., Ruan, J., Yin, Q., Atianand, M.K., Vos, M.R., Schroder, G.F., Fitzgerald, K.A., Wu, H., and Egelman, E.H. (2014). Unified polymerization mechanism for the assembly of ASC-dependent inflammasomes. Cell *156*, 1193-1206.

Mantovani, A., Biswas, S.K., Galdiero, M.R., Sica, A., and Locati, M. (2013). Macrophage plasticity and polarization in tissue repair and remodelling. J Pathol *229*, 176-185.

Mariathasan, S., and Monack, D.M. (2007). Inflammasome adaptors and sensors: intracellular regulators of infection and inflammation. Nat Rev Immunol *7*, 31-40.

Martinon, F., Burns, K., and Tschopp, J. (2002). The inflammasome: a molecular platform triggering activation of inflammatory caspases and processing of proIL-beta. Mol Cell *10*, 417-426.

Miao, E.A., Leaf, I.A., Treuting, P.M., Mao, D.P., Dors, M., Sarkar, A., Warren, S.E., Wewers, M.D., and Aderem, A. (2010). Caspase-1-induced pyroptosis is an innate immune effector mechanism against intracellular bacteria. Nat Immunol *11*, 1136-1142.

Morimoto, N., Kono, T., Sakai, M., and Hikima, J.I. (2021). Inflammasomes in Teleosts: Structures and Mechanisms That Induce Pyroptosis during Bacterial Infection. Int J Mol Sci *22*.

Nambayan, R.J.T., Sandin, S.I., Quint, D.A., Satyadi, D.M., and de Alba, E. (2019). The inflammasome adapter ASC assembles into filaments with integral participation of its two Death Domains, PYD and CARD. J Biol Chem *294*, 439-452.

Nguyen-Chi, M., Laplace-Builhe, B., Travnickova, J., Luz-Crawford, P., Tejedor, G., Phan, Q.T., Duroux-Richard, I., Levraud, J.P., Kissa, K., Lutfalla, G.*, et al.* (2015). Identification of polarized macrophage subsets in zebrafish. Elife *4*, e07288.

Patel, U., Rajasingh, S., Samanta, S., Cao, T., Dawn, B., and Rajasingh, J. (2017). Macrophage polarization in response to epigenetic modifiers during infection and inflammation. Drug Discov Today *22*, 186-193.

Pfaffl, M.W. (2001). A new mathematical model for relative quantification in real-time RT-PCR. Nucleic Acids Res *29*, e45.

Phan, Q.T., Sipka, T., Gonzalez, C., Levraud, J.P., Lutfalla, G., and Nguyen-Chi, M. (2018). Neutrophils use superoxide to control bacterial infection at a distance. PLoS Pathog *14*, e1007157.

Renshaw, S.A., Loynes, C.A., Trushell, D.M., Elworthy, S., Ingham, P.W., and Whyte, M.K. (2006). A transgenic zebrafish model of neutrophilic inflammation. Blood *108*, 3976-3978.

Schindelin, J., Arganda-Carreras, I., Frise, E., Kaynig, V., Longair, M., Pietzsch, T., Preibisch, S., Rueden, C., Saalfeld, S., Schmid, B.*, et al.* (2012). Fiji: an open-source platform for biological-image analysis. Nat Methods *9*, 676-682.

Schroder, K., and Tschopp, J. (2010). The inflammasomes. Cell *140*, 821-832.

Shapouri-Moghaddam, A., Mohammadian, S., Vazini, H., Taghadosi, M., Esmaeili, S.A., Mardani, F., Seifi, B., Mohammadi, A., Afshari, J.T., and Sahebkar, A. (2018). Macrophage plasticity, polarization, and function in health and disease. Journal of cellular physiology *233*, 6425-6440.

Shenoy, A.R., Wellington, D.A., Kumar, P., Kassa, H., Booth, C.J., Cresswell, P., and MacMicking, J.D. (2012). GBP5 promotes NLRP3 inflammasome assembly and immunity in mammals. Science *336*, 481-485.

Sollberger, G., Choidas, A., Burn, G.L., Habenberger, P., Di Lucrezia, R., Kordes, S., Menninger, S., Eickhoff, J., Nussbaumer, P., Klebl, B.*, et al.* (2018). Gasdermin D plays a vital role in the generation of neutrophil extracellular traps. Sci Immunol *3*.

Su, Y., Gao, J., Kaur, P., and Wang, Z. (2020). Neutrophils and Macrophages as Targets for Development of Nanotherapeutics in Inflammatory Diseases. Pharmaceutics *12*.

Thomas, C.J., and Schroder, K. (2013). Pattern recognition receptor function in neutrophils. Trends Immunol *34*, 317-328.

Tyrkalska, S.D., Candel, S., Angosto, D., Gomez-Abellan, V., Martin-Sanchez, F., Garcia-Moreno, D., Zapata-Perez, R., Sanchez-Ferrer, A., Sepulcre, M.P., Pelegrin, P.*, et al.* (2016).

Neutrophils mediate Salmonella Typhimurium clearance through the GBP4 inflammasome-dependent production of prostaglandins. Nat Commun *7*, 12077.

Tyrkalska, S.D., Candel, S., and Mulero, V. (2021). The neutrophil inflammasome. Dev Comp Immunol *115*, 103874.

Tyrkalska, S.D., Martinez-Lopez, A., Arroyo, A.B., Martinez-Morcillo, F.J., Candel, S., Garcia-Moreno, D., Mesa-Del-Castillo, P., Cayuela, M.L., and Mulero, V. (2022). Differential proinflammatory activities of Spike proteins of SARS-CoV-2 variants of concern. Sci Adv *8*, eabo0732.

Tyrkalska, S.D., Martinez-Lopez, A., Pedoto, A., Candel, S., Cayuela, M.L., and Mulero, V. (2023a). The Spike protein of SARS-CoV-2 signals via Tlr2 in zebrafish. Dev Comp Immunol *140*, 104626.

Tyrkalska, S.D., Pedoto, A., Martinez-Lopez, A., Ros-Lucas, J.A., Mesa-Del-Castillo, P., Candel, S., and Mulero, V. (2023b). Silica crystals activate toll-like receptors and inflammasomes to promote local and systemic immune responses in zebrafish. Dev Comp Immunol *138*, 104523.

Tyrkalska, S.D., Perez-Oliva, A.B., Rodriguez-Ruiz, L., Martinez-Morcillo, F.J., Alcaraz-Perez, F., Martinez-Navarro, F.J., Lachaud, C., Ahmed, N., Schroeder, T., Pardo-Sanchez, I.*, et al.* (2019). Inflammasome Regulates Hematopoiesis through Cleavage of the Master Erythroid Transcription Factor GATA1. Immunity *51*, 50-63 e55.

Van Gorp, H., Van Opdenbosch, N., and Lamkanfi, M. (2019). Inflammasome-Dependent Cytokines at the Crossroads of Health and Autoinflammatory Disease. Cold Spring Harb Perspect Biol *11*.

Varol, C., Mildner, A., and Jung, S. (2015). Macrophages: development and tissue specialization. Annual review of immunology *33*, 643-675.

von Moltke, J., Trinidad, N.J., Moayeri, M., Kintzer, A.F., Wang, S.B., van Rooijen, N., Brown, C.R., Krantz, B.A., Leppla, S.H., Gronert, K.*, et al.* (2012). Rapid induction of inflammatory lipid mediators by the inflammasome in vivo. Nature *490*, 107-111.

Walton, E.M., Cronan, M.R., Beerman, R.W., and Tobin, D.M. (2015). The Macrophage-Specific Promoter mfap4 Allows Live, Long-Term Analysis of Macrophage Behavior during Mycobacterial Infection in Zebrafish. PLoS One *10*, e0138949.

Wang, C., Yang, T., Xiao, J., Xu, C., Alippe, Y., Sun, K., Kanneganti, T.D., Monahan, J.B., Abu-Amer, Y., Lieberman, J.*, et al.* (2021). NLRP3 inflammasome activation triggers gasdermin D-independent inflammation. Sci Immunol *6*, eabj3859.

Weinberg, J.M., Bienholz, A., and Venkatachalam, M.A. (2016). The role of glycine in regulated cell death. Cell Mol Life Sci *73*, 2285-2308.

Westerfield, M. (2000). The Zebrafish Book. A Guide for the Laboratory Use of Zebrafish Danio* (Brachydanio) rerio. (Eugene, OR: University of Oregon Press).

White, R.M., Sessa, A., Burke, C., Bowman, T., LeBlanc, J., Ceol, C., Bourque, C., Dovey, M., Goessling, W., Burns, C.E.*, et al.* (2008). Transparent adult zebrafish as a tool for in vivo transplantation analysis. Cell Stem Cell *2*, 183-189.

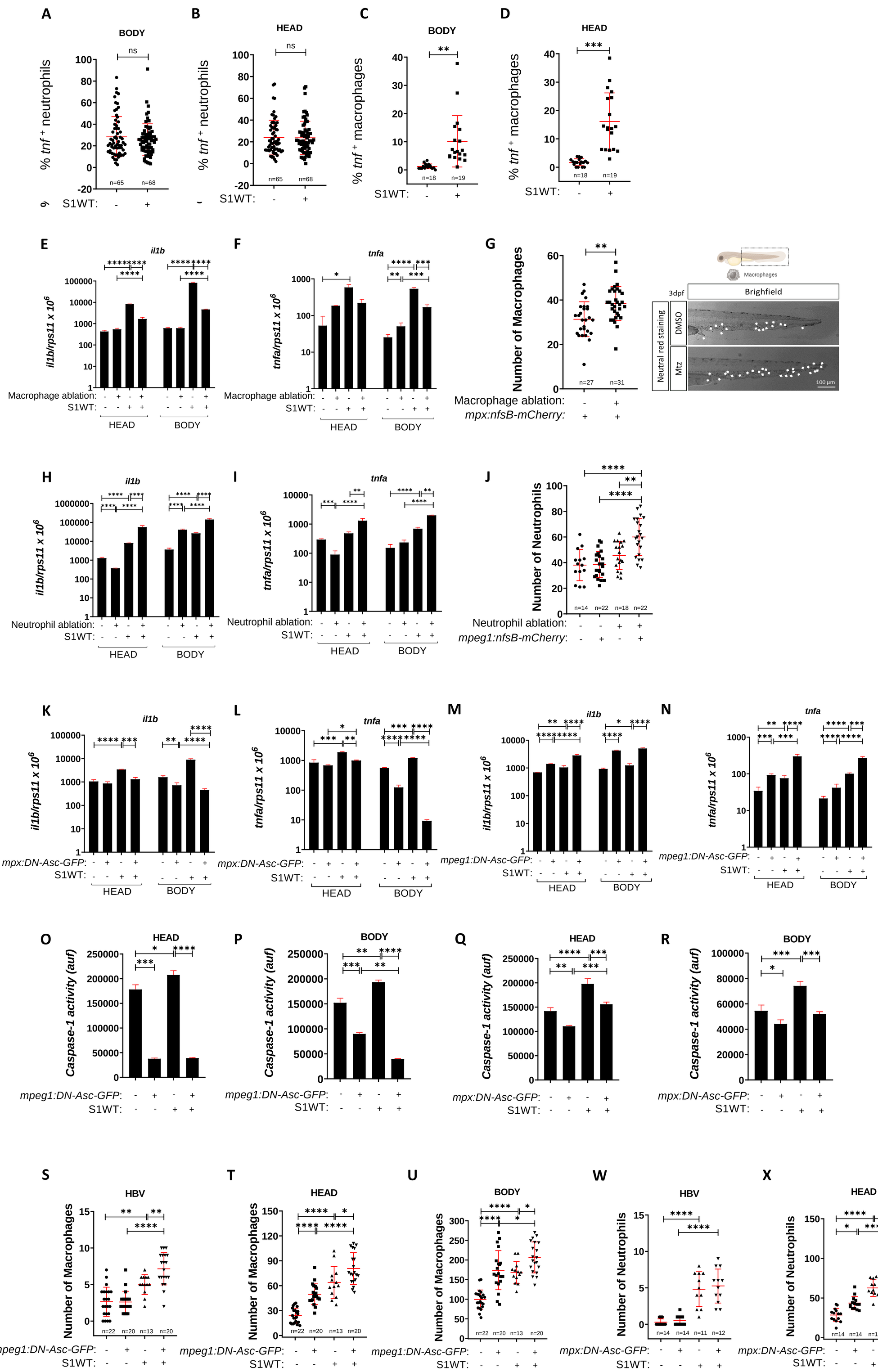

Figure 1. Inhibition of the macrophage inflammasome exacerbates inflammation in a COVID19-associated CSS model. Recombinant S1WT (+) or vehicle (−) were injected in the hindbrain ventricle (HBV) of 2-day postfertilization (dpf) *Tg(lyz:DsRED2)* and *Tg(tnfa:eGFP)* (A, B), Tg*(mfap4:tomato)* and *Tg(tnfa:eGFP)* (C, D), *Tg(mpx:GAL4)* and *Tg(UAS:nfsB-mCherry)* (E, F, G), Tg(mpeg1:GAL4) and Tg(UAS:nfsB-mCherry) (H, I), Tg(mpeg1:GAL4:mfap4:tomato) and Tg(UAS:nfsB-mCherry) (J), Tg(mpx:GAL4) and Tg(UAS:ascΔCARD-GFP) (K, L, Q, R), *Tg(mpeg1:GAL4)* and *Tg(UAS:DN-asc-GFP)* (M, N, O, P), *Tg(mpeg1:GAL4, mfap4:tomato)* and *Tg(UAS:DN-asc-GFP)* (S, T, U*), Tg(mpx:GAL4:lyz:DsRED2)* and *Tg(UAS:DN-asc-GFP)* (W, X, Y) larvae. The larvae were treated with 5 mM Metronidazole for specific cell ablation during 48 h (E, F, G, H, I, J). The percentage of *tnfa*+ neutrophils (A, B) and macrophages (C, D) were analyzed at 6 hpi using a fluorescence microscope. The transcript levels of the indicated genes (E, F, H, I, K, L, M, N) were analyzed at 12 hpi by RT-qPCR in larval head and tail. Macrophage (G, S, T, U) and neutrophil (J, W, X, Y) number and their recruitment were analyzed at 6 hpi by fluorescence microscopy or neutral red staining. Caspase-1 activity was determined at 24 hpi using a fluorogenic substrate (O, P, Q, R). Each dot represents one individual, and the means ± SEM for each group is also shown. P values were calculated using Student´s t-test or one-way analysis of variance (ANOVA) and Tukey multiple range test. *P ≤ 0.05, **P ≤ 0.01, ***P ≤ 0.001, and ****P ≤ 0.0001. auf, arbitrary units of fluorescence. Scale bars 100 µm.

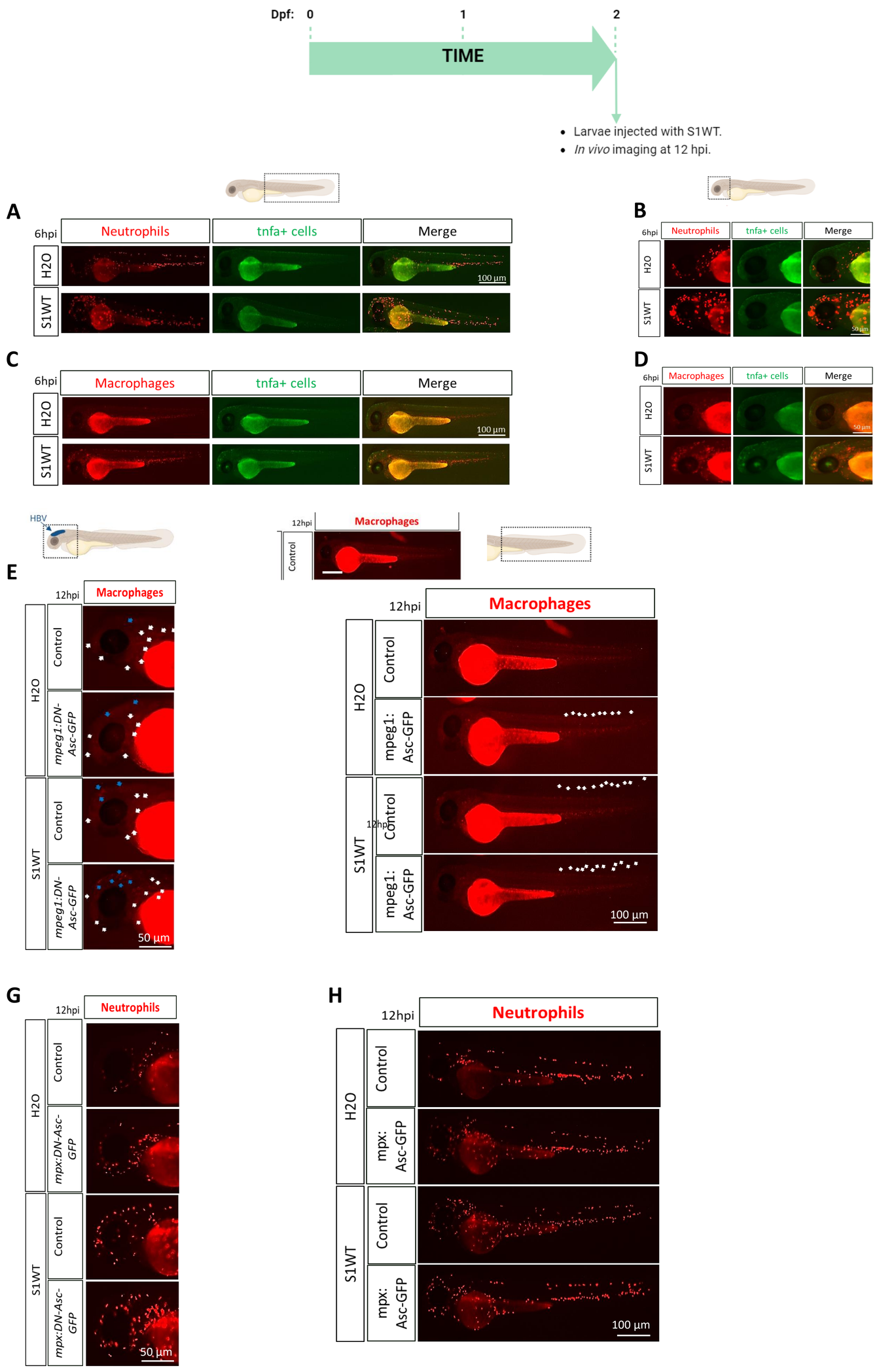

Figure S1 (related to Figure 1). Representative green and red fluorescence images of larvae of the different groups shown in Figure 1. Recombinant S1WT or vehicle (-) were injected in the hindbrain ventricle (HBV) of 2 dpf *Tg(lyz:DsRED2)* and *Tg(tnfa:eGFP)* (A, B), *Tg(mfap4:tomato)* and *Tg(tnfa:eGFP)* (C, D), *Tg(mpeg1:GAL4, mfap4:tomato)* and *Tg(UAS:DN-asc-GFP)* (E, F), *Tg(mpx:GAL4:lyz:DsRED2)* and *Tg(UAS:DN-asc-GFP)* (G, H) larvae. Neutrophils in the body (A, H) and in the HBV and head (B, G), and macrophages in the body (C, F) and in the HBV and head (D, E) visualized at 6 or 12 hpi by fluorescence microscopy. The regions of interest used for quantification in all experiments are indicated in the schematic representation of the larva. Bars: 100 µm (whole larva) and 50 µm (head).

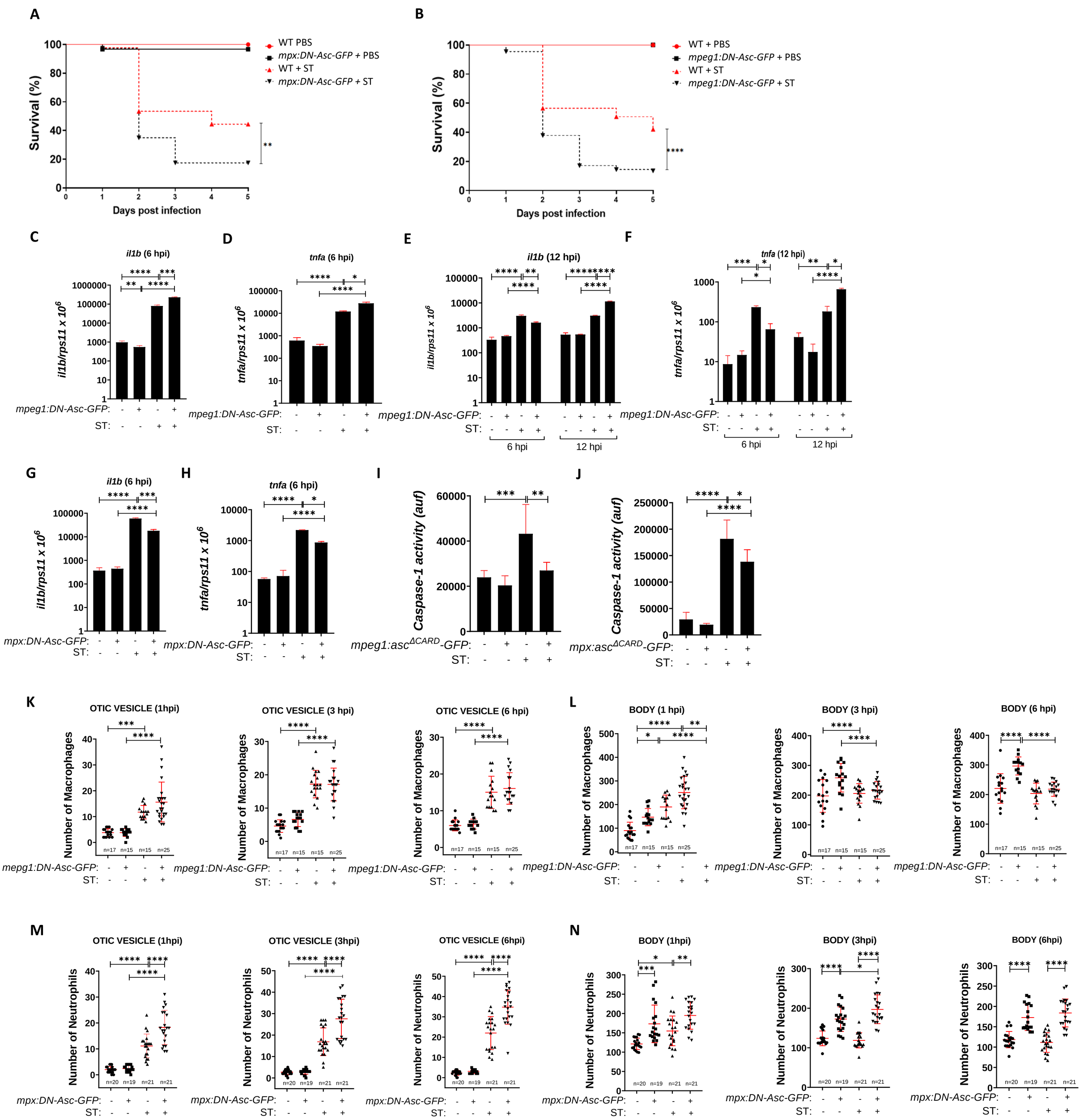

Figure 2. Inhibition of the macrophage inflammasome exacerbates inflammation in a zebrafish infection model. *Tg(mpx:GAL4)* and *Tg(UAS:DN-asc-GFP)* (A) and *Tg(mpeg1:GAL4)* and *Tg(UAS:DN-asc-GFP)* (B) zebrafish larvae were dechorionated and infected at 2 dpf via the yolk sac with wild-type strain of ST, and the number of surviving larvae counted daily during the next 5 days. ST was injected in the yolk sac of 2 dpf *Tg(mpeg1:GAL4)* and *Tg(UAS:DN-asc-GFP)* (C, D, E, F, I) and *Tg(mpx:GAL4)* and *Tg(UAS:DN-asc-GFP)* (G, H, J) larvae and in the otic vesicle of 2 dpf Tg(mpeg1:GAL4:mfap4:tomato) and *Tg(UAS:DN-asc-GFP)* (K, L), *Tg(mpx:GAL4:lyz:DsRED2)* and *Tg(UAS:DN-asc-GFP)* (M, N) larvae. The transcript levels of the indicated genes (C, D, E, F, G, H) were analyzed at 6, 12 or 24 hpi by RT-qPCR in larval head and tail. Macrophage (K, L) and neutrophil (M, N) number and recruitment were analyzed at 1, 3, and 6 hpi by fluorescence microscopy. Caspase-1 activity was determined at 24 hpi using a fluorogenic substrate (I, J). Each dot represents one individual, and the means ± SEM for each group is also shown. P values were calculated using one-way analysis of variance (ANOVA) and Tukey multiple range test. *P ≤ 0.05, **P ≤ 0.01, ***P ≤ 0.001, and ****P ≤ 0.0001. auf, arbitrary units of fluorescence.

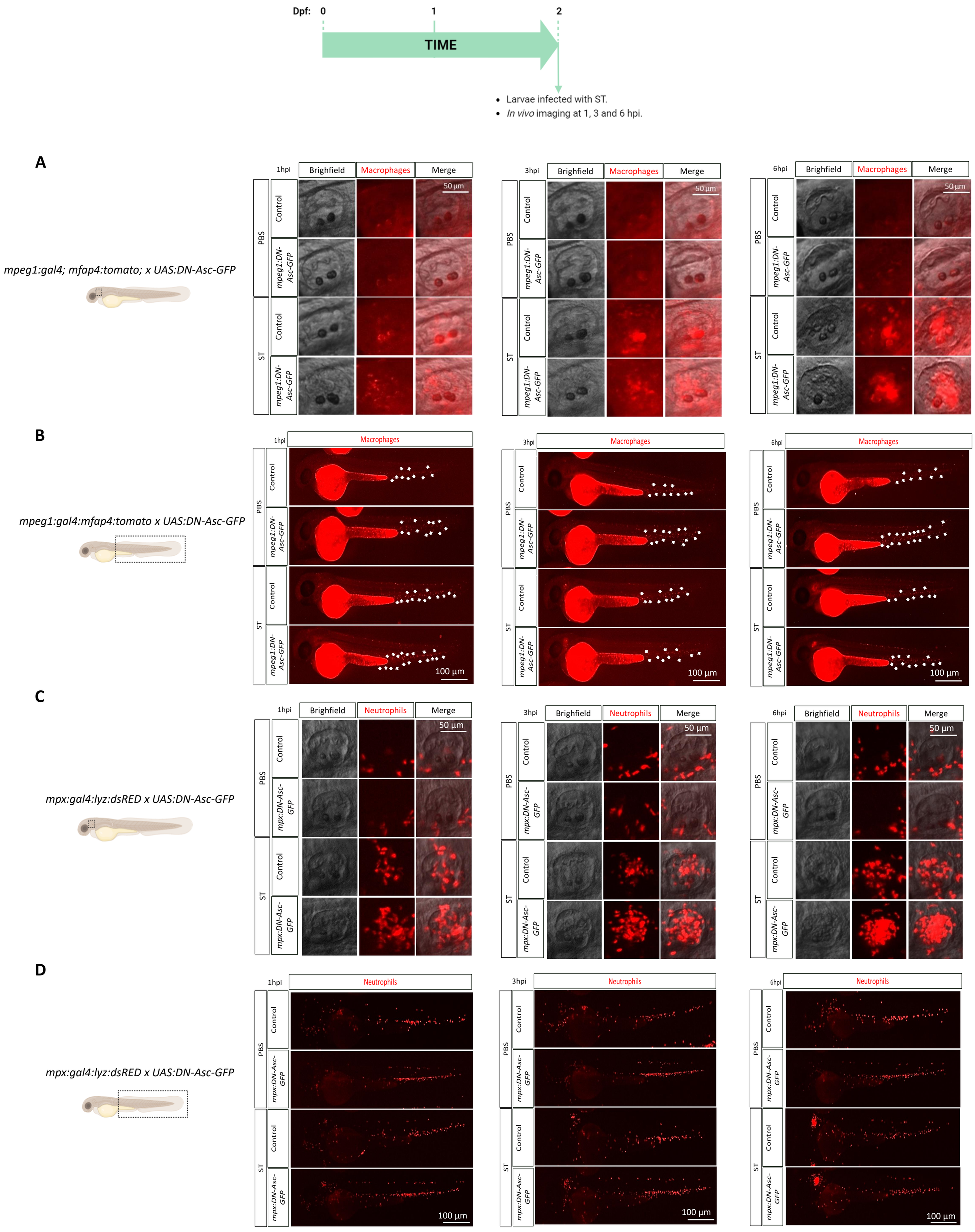

Figure S2 (related to Figure 2). Representative red fluorescent images of larvae of the different groups shown in Figure 2. ST was injected in the otic vesicle of 2 dpf *Tg(mpeg1:GAL4, mfap4:tomato)* and *Tg(UAS:DN-asc-GFP)* (A, B), *Tg(mpx:GAL4:lyz:DsRED2)* and *Tg(UAS:DN-asc-GFP)* (C, D) larvae. Macrophages in the otic vesicle (A) and in the body (B), and neutrophils in the otic vesicle (C) and in the body (D) were visualized at 1, 3 and 6 hpi by fluorescence microscopy. The regions of interest used for quantification in all experiments are indicated in the schematic representation of the larvae. Bars: 100 µm (whole larva) and 50 µm (otic vesicle). .

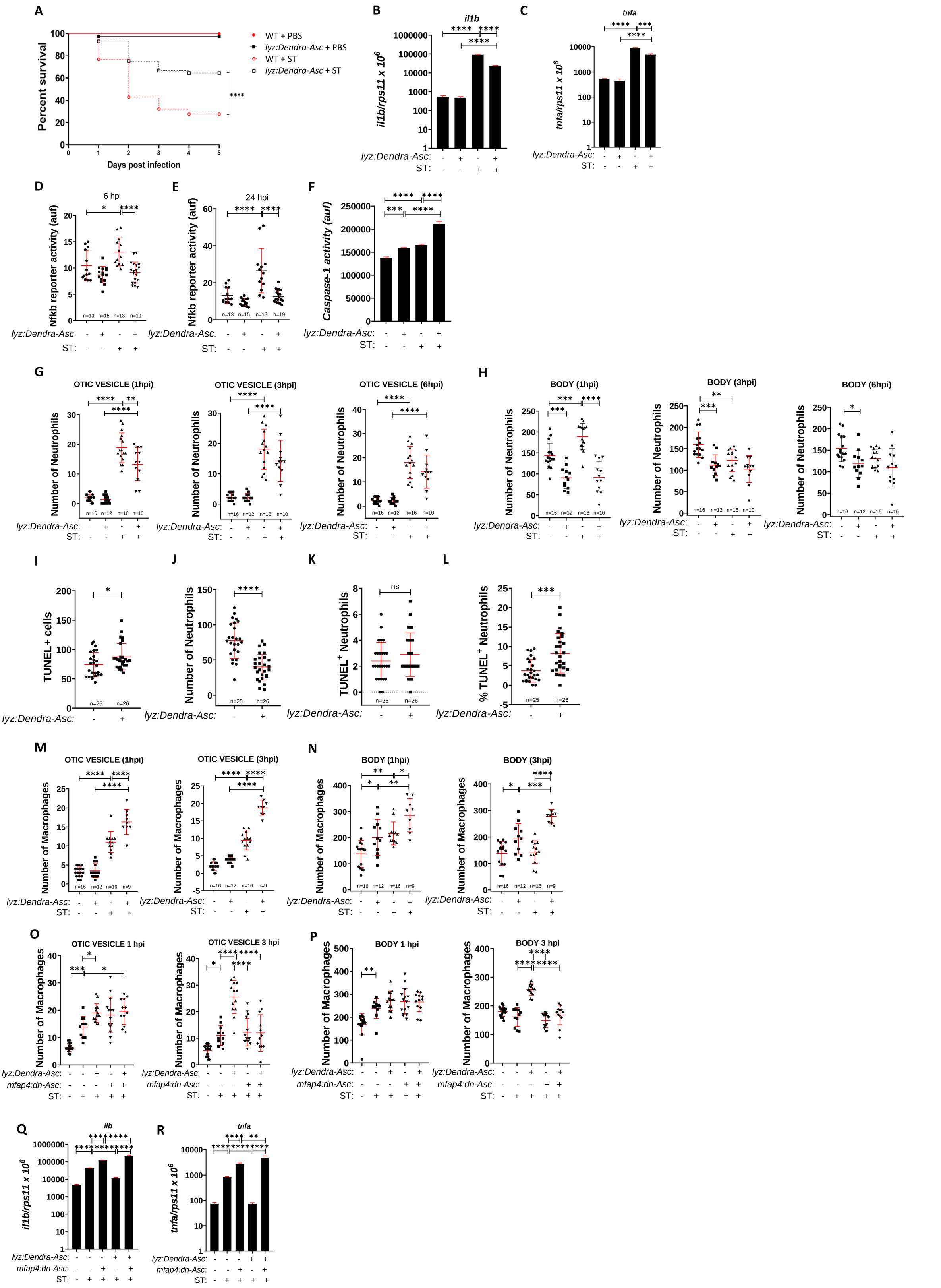

Figure 3. Overactivation of neutrophil inflammasome leads to myeloid cell imbalance and attenuated inflammation. *Tg(lyz:Dendra-Asc)* (A, B, C, F) and *Tg(lyz:Dendra-Asc)* and *Tg(nfkb:eGFP)* (D, E), *Tg(lyz:Dendra-Asc)* and *Tg(lyz:DsRED2)* (G, H), *Tg(lyz:Dendra-Asc)* and *Tg(mfap4:tomate)* (M, N), *Tg(lyz:Dendra-Asc)* and *Tg(mpx:eGFP)* (I, J, K, L) were used. Embryos were infected in yolk sac (A, B, C, D, E, F Q, R) or in the otic vesicle with wild-type strain of ST (G, H, M, N, O, P). Zebrafish one-cell embryos were injected with *mfap4:DN-Asc* plasmid (O, P, Q, R). The number of surviving larvae counted daily during the next 5 days were analyzed (A). The transcript levels of the indicated genes (B, C, Q, R) were analyzed at 24 hpi by RT-qPCR in whole larvae. NfkB activation (D, E) was analyzed at 6 and 24 hpi using a fluorescence microscope. Neutrophil (G, H) and macrophage (M, N, O, P) number and recruitment were analyzed at 1, 3, 6, and 24 hpi by fluorescence microscopy. TUNEL assay and immunohistochemistry staining (I, J, K, L) were performed. Caspase-1 activity was determined at 24 hpi using a fluorogenic substrate (F). Each dot represents one individual, and the means ± SEM for each group is also shown. P values were calculated using Studet´s t-test or one-way analysis of variance (ANOVA) and Tukey multiple range test. *P ≤ 0.05, **P ≤ 0.01, ***P ≤ 0.001, and ****P ≤ 0.0001. auf, arbitrary units of fluorescence.

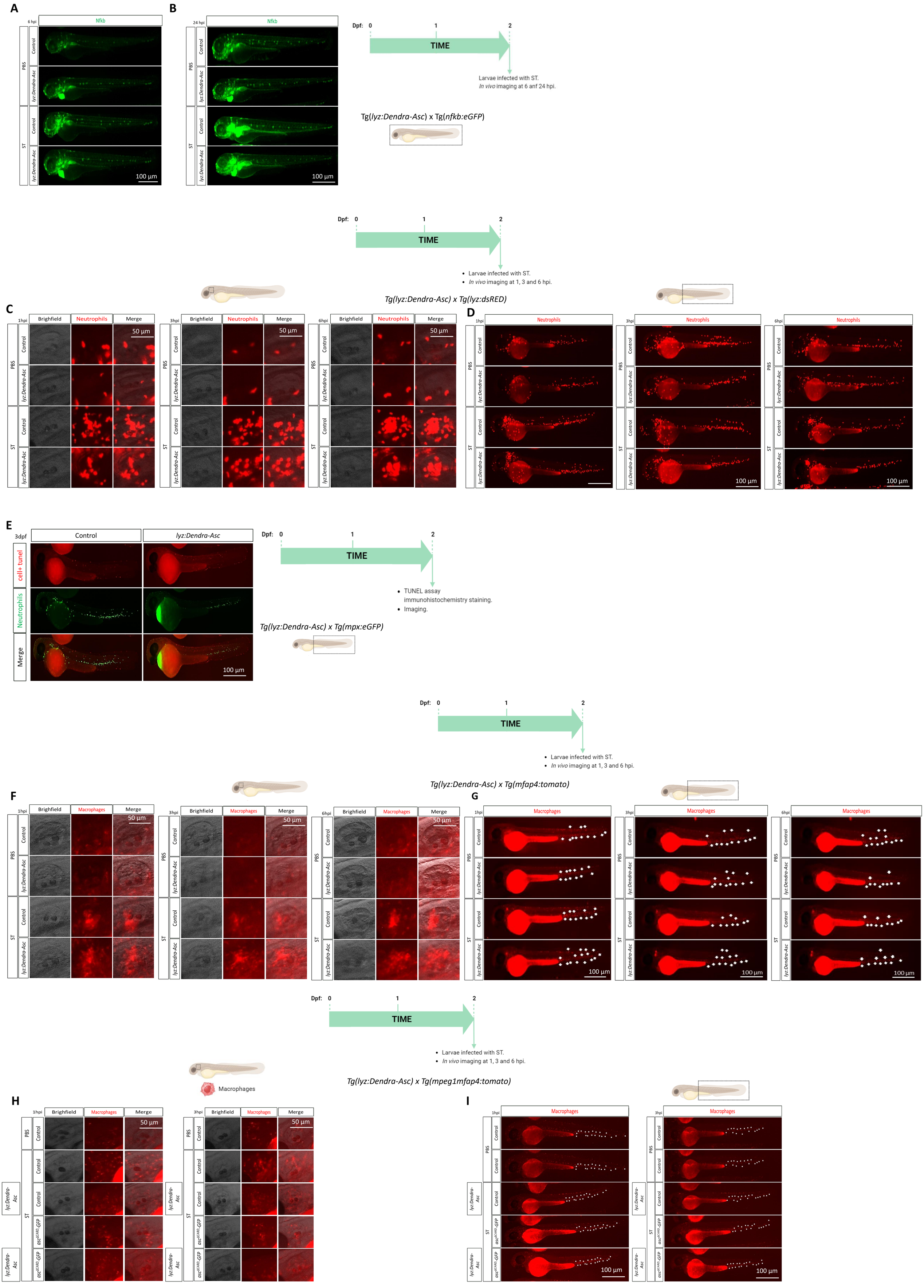

Figure S3 (related to Figure 3). Representative green and red fluorescence images of larvae of the different groups shown in Figure 3. ST was injected in the yolk sac of 2 dpf *Tg(lyz:Dendra-Asc)* and *Tg(nfkb:eGFP)* (A, B), and in the otic vesicle of 2 dpf *Tg(lyz:Dendra-Asc)* and *Tg(lyz:DsRED2)* (C, D), *Tg(lyz:Dendra-Asc)* and *Tg(mfap4:tomato)* (F, G, H, I), larvae. Neutrophils in the otic vesicle (C) and in the body (D), and macrophages in the otic vesicle (F, H) and in the body (G, I) were visualized at 1, 3 and 6 hpi by fluorescence microscopy. The number of neutrophils and the number of TUNEL positive cells (E) were quantified using a fluorescence microscopy. The regions of interest used for quantitation in all experiments are indicated in the schematic representation of the larvae. Bars: 100 µm (whole larva) and 50 µm (otic vesicle).

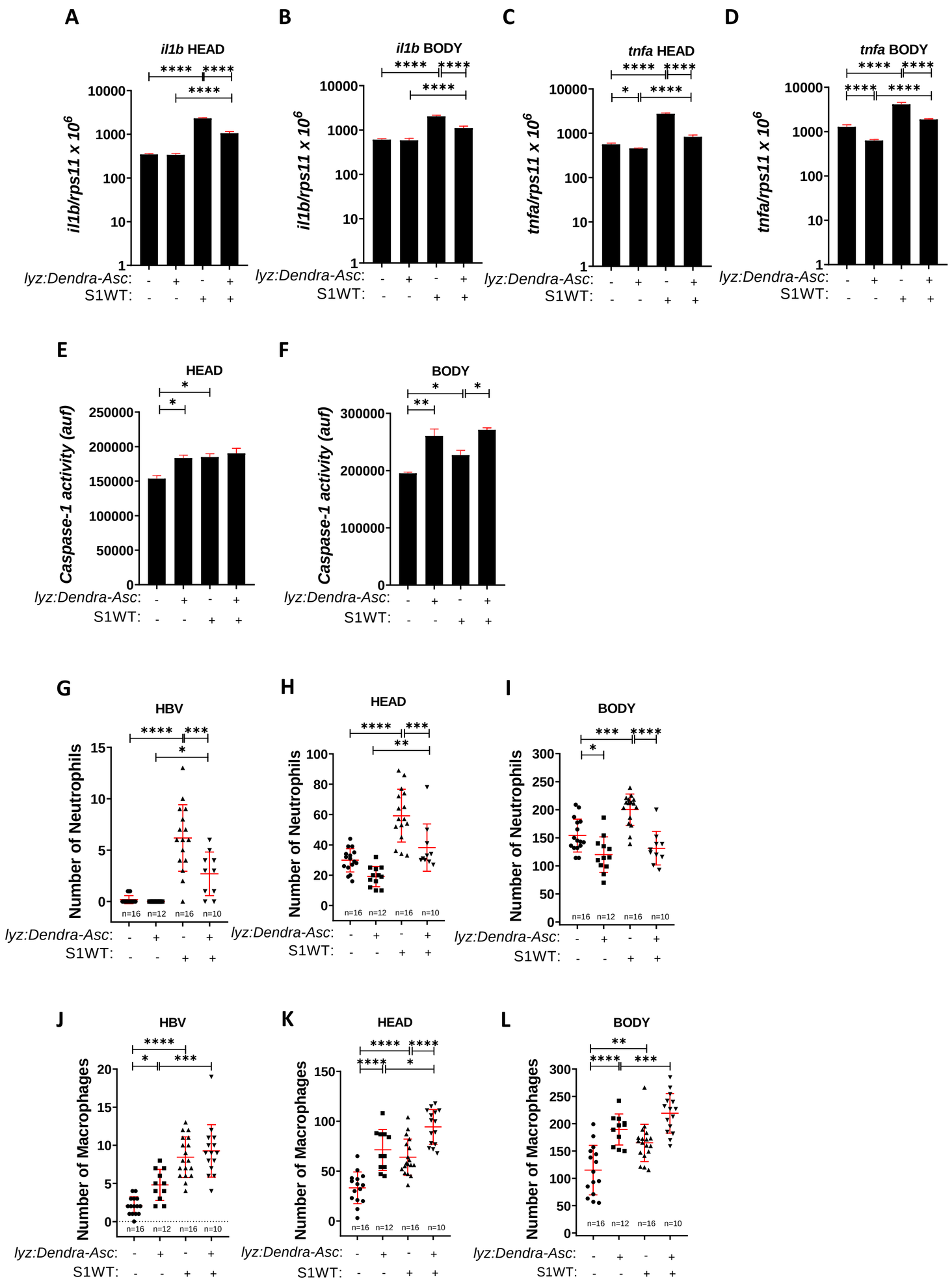

Figure S4 (related to Fig. 3). Recombinant S1WT (+) or vehicle (−) were injected in the hindbrain ventricle (HBV) of 2-day postfertilization (dpf) *Tg(lyz:Dendra-Asc)* (A, B, C, D, E, F). *Tg(lyz:Dendra-Asc)* and *Tg(lyz:DsRED2)* (G, H, I), *Tg(lyz:Dendra-Asc*) and *Tg(mfap4:tomato)* (J, K, L) larvae. The transcript levels of the indicated genes (A, B, C, D) were analyzed at 24 hpi by RT-qPCR in larval head and tail. Neutrophil (G, H, I) and macrophage (J, K, L) number and their recruitment were analyzed at 6 hpi by fluorescence microscopy. Caspase-1 activity was determined at 24 hpi using a fluorogenic substrate (E, F). Each dot represents one individual, and the means ± SEM for each group is also shown. P values were calculated using one-way analysis of variance (ANOVA) and Tukey multiple range test. *P ≤ 0.05, **P ≤ 0.01, ***P ≤ 0.001, and ****P ≤ 0.0001. auf, arbitrary units of fluorescence.

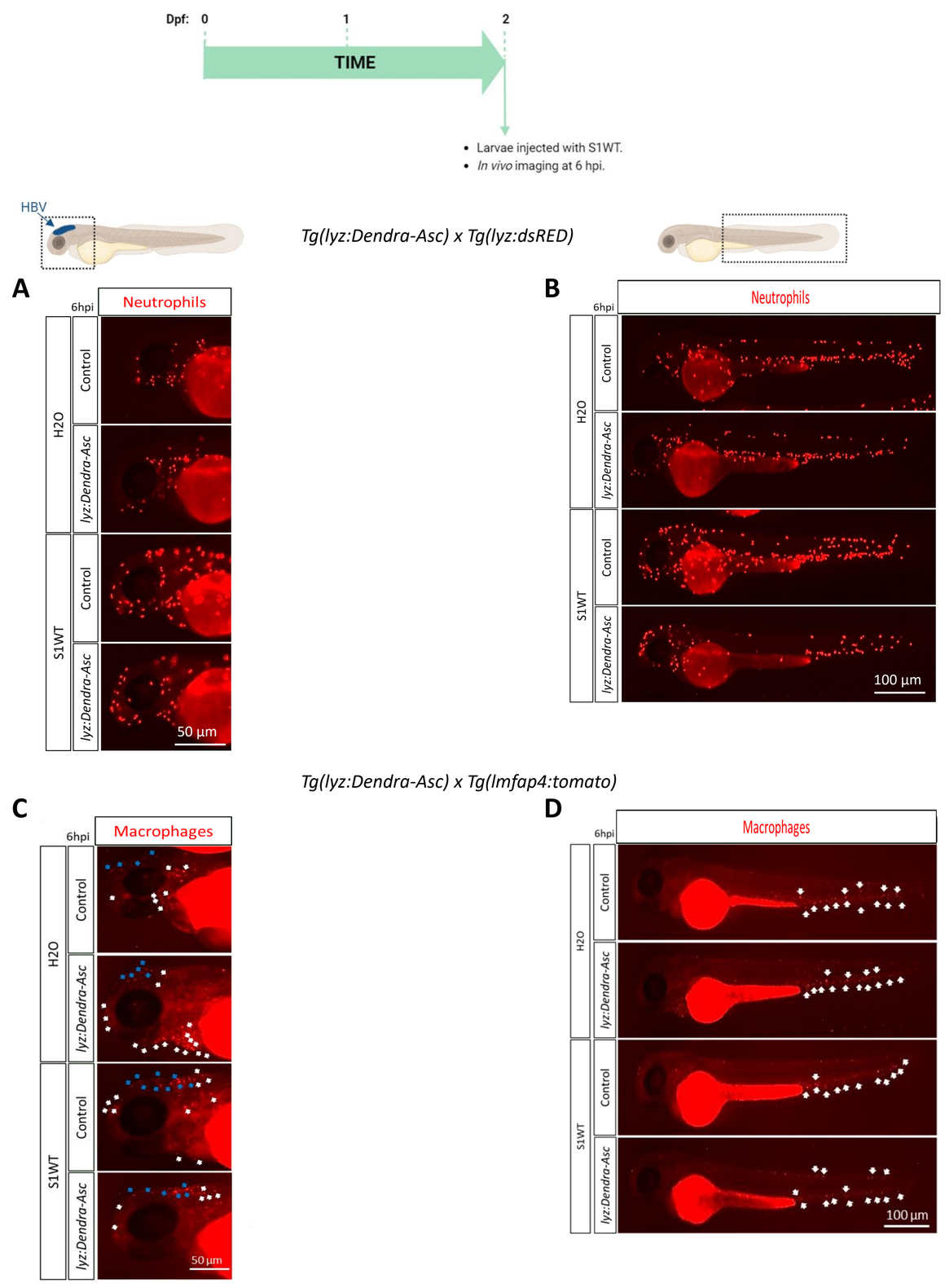

Figure S5 (related to Figure 3). Representative red fluorescence images of larvae of the different groups shown in Figures S4. Recombinant S1WT or vehicle (-) were injected in the hindbrain ventricle (HBV) of 2 dpf *Tg(lyz:Dendra-Asc)* and *Tg(lyz:DsRED2)* (A, B), *Tg(lyz:Dendra-Asc)* and *Tg(mfap4:tomato)* (C, D) larvae. Neutrophils in the head (A) and in the body (B), and macrophages in the head (C) and in the body (D) visualized at 6 hpi by fluorescence microscopy. The regions of interest used for quantification in all experiments are indicated in the schematic representation of the larvae. Bars: 100 µm (whole larva) and 50 µm (head).

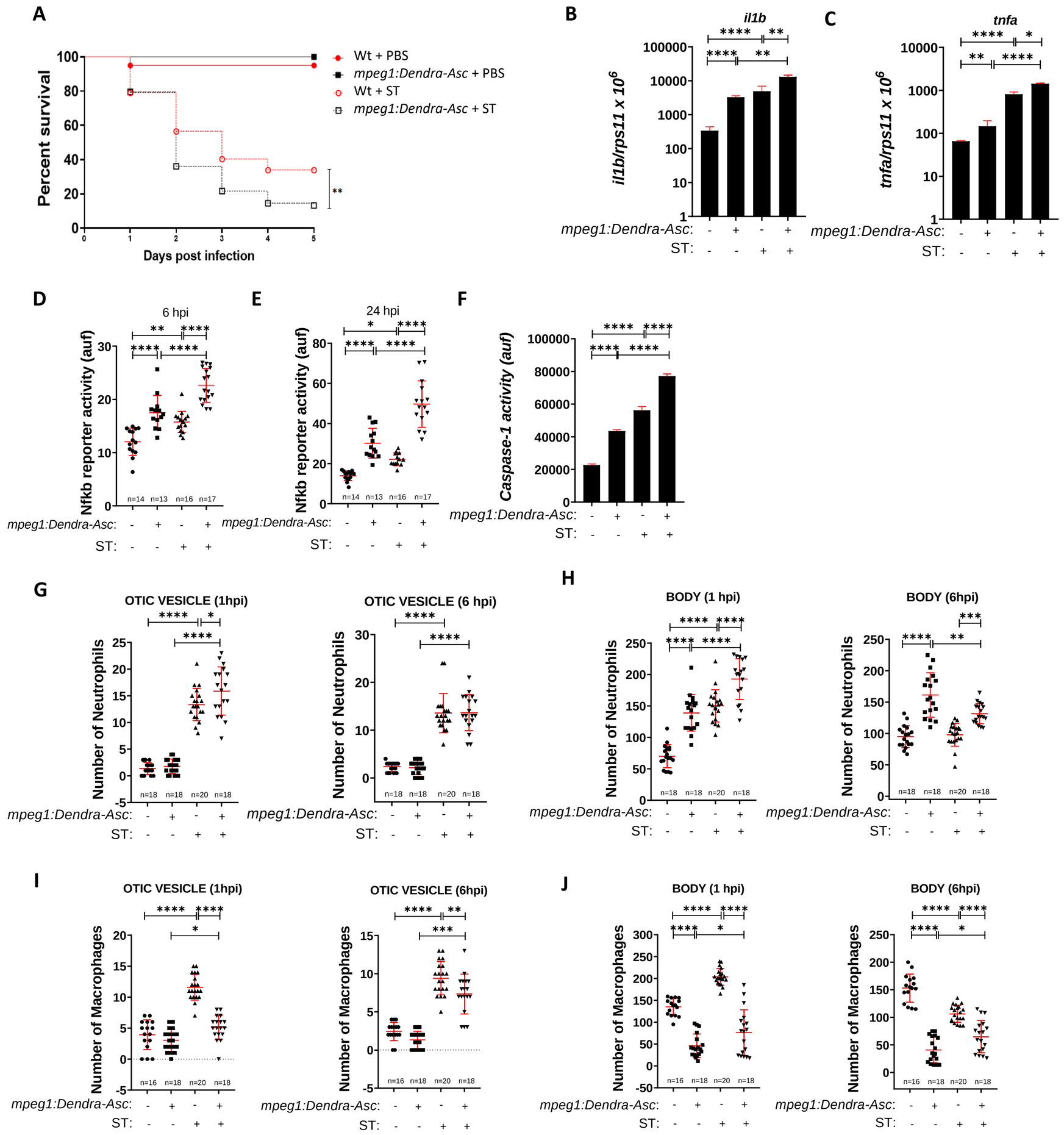

Figure 4. Overactivation of the macrophage inflammasome leads to myeloid cell imbalance and enhanced inflammation in ST infection model. Zebrafish one-cell embryos were injected with *mpeg1:Dendra-Asc* plasmid (A-J). ST was then injected in the yolk sac of 2dpf wild-type larvae (A, B, C, F), *Tg(nfkb:eGFP)* (D, E), or in the otic vesicle of *Tg(mpx:eGFP)* (G, H) and *Tg(mpeg1:mCherry)* (I, J) larvae. The number of surviving larvae were analyzed daily during the next 5 days (A). The transcript levels of the indicated genes (B, C) were analyzed at 24 hpi by RT-qPCR. NfkB activation was analyzed at 6 and 24 hpi (D, E). Caspase-1 activity was determined at 24 hpi using a fluorogenic substrate (F). Neutrophil (G, H) and macrophage (I, J) number and recruitment were analyzed at 1, 3, and 6 hpi by fluorescence microscopy. Each dot represents one individual, and the means ± SEM for each group is also shown. P values were calculated using one-way analysis of variance (ANOVA) and Tukey multiple range test. *$P \leq 0.05$, **$P \leq 0.01$, ***$P \leq 0.001$, and ****$P \leq 0.0001$. auf, arbitrary units of fluorescence.

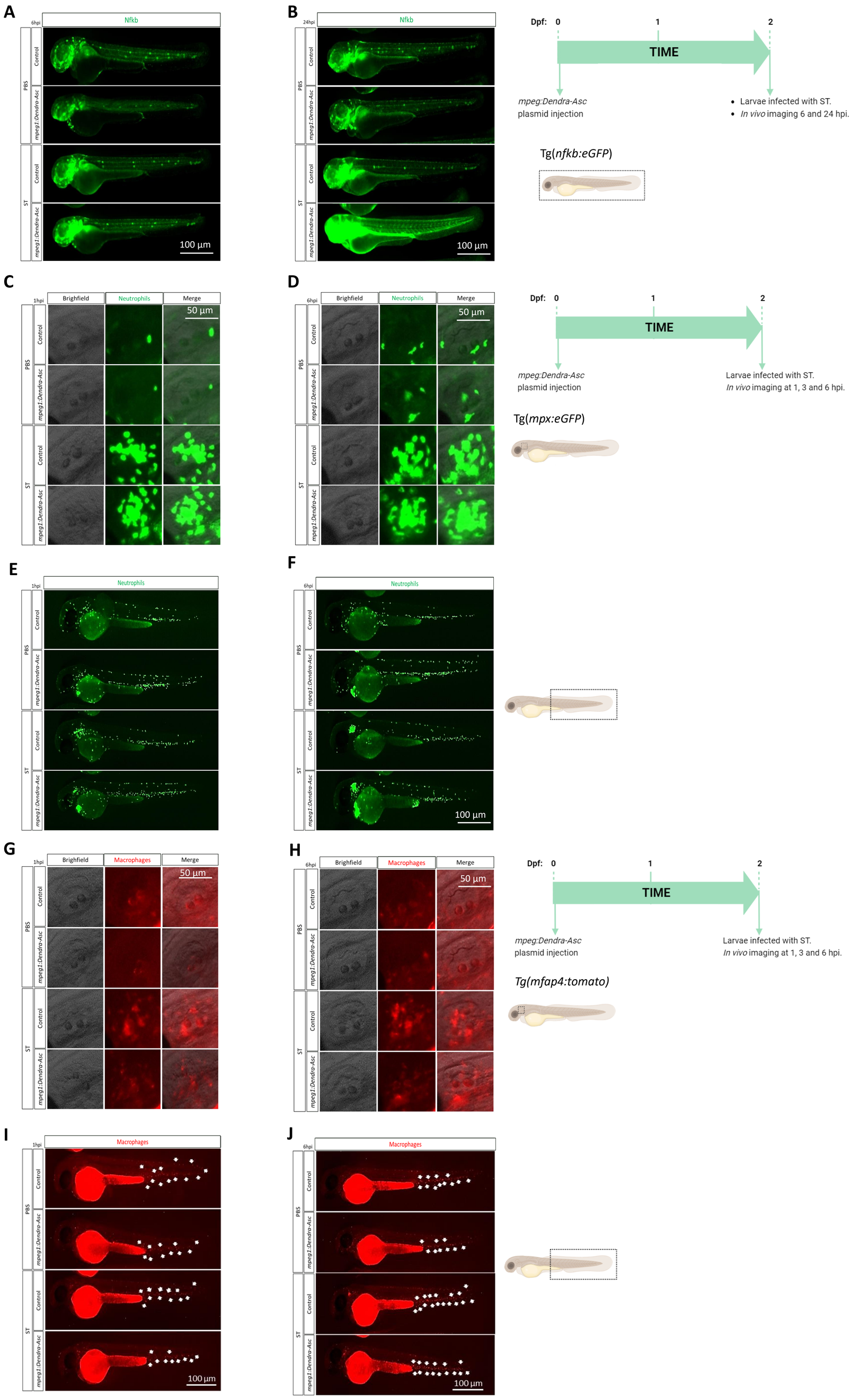

Figure S6 (related to Figure 4). Representative green and red fluorescence images of larvae of the different groups shown in Figures 4. Zebrafish one-cell stage embryos were injected with *mpeg1:Dendra-Asc* plasmid and infected with ST in the yolk sac of 2 dpf *Tg(nfkb:eGFP)* (A, B) and in the otic vesicle of 2 dpf *Tg(mpx:eGFP)* (C, D, E, F), *Tg(mfap4:tomato)* (G, H, I, J) larvae. Nfkb activity (A, B) was visualized at 6 and 24 hpi by fluorescence microscopy. Neutrophils in the otic vesicle (C, D) and in the body (E, F), and macrophages in the otic vesicle (G, H) and in the body (I, J) were visualized at 1, 3, 6 hpi by fluorescence microscopy. The regions of interest used for quantification in all experiments are indicated in the schematic representation of the larvae. Bars: 100 µm (whole larva) and 50 µm (head).

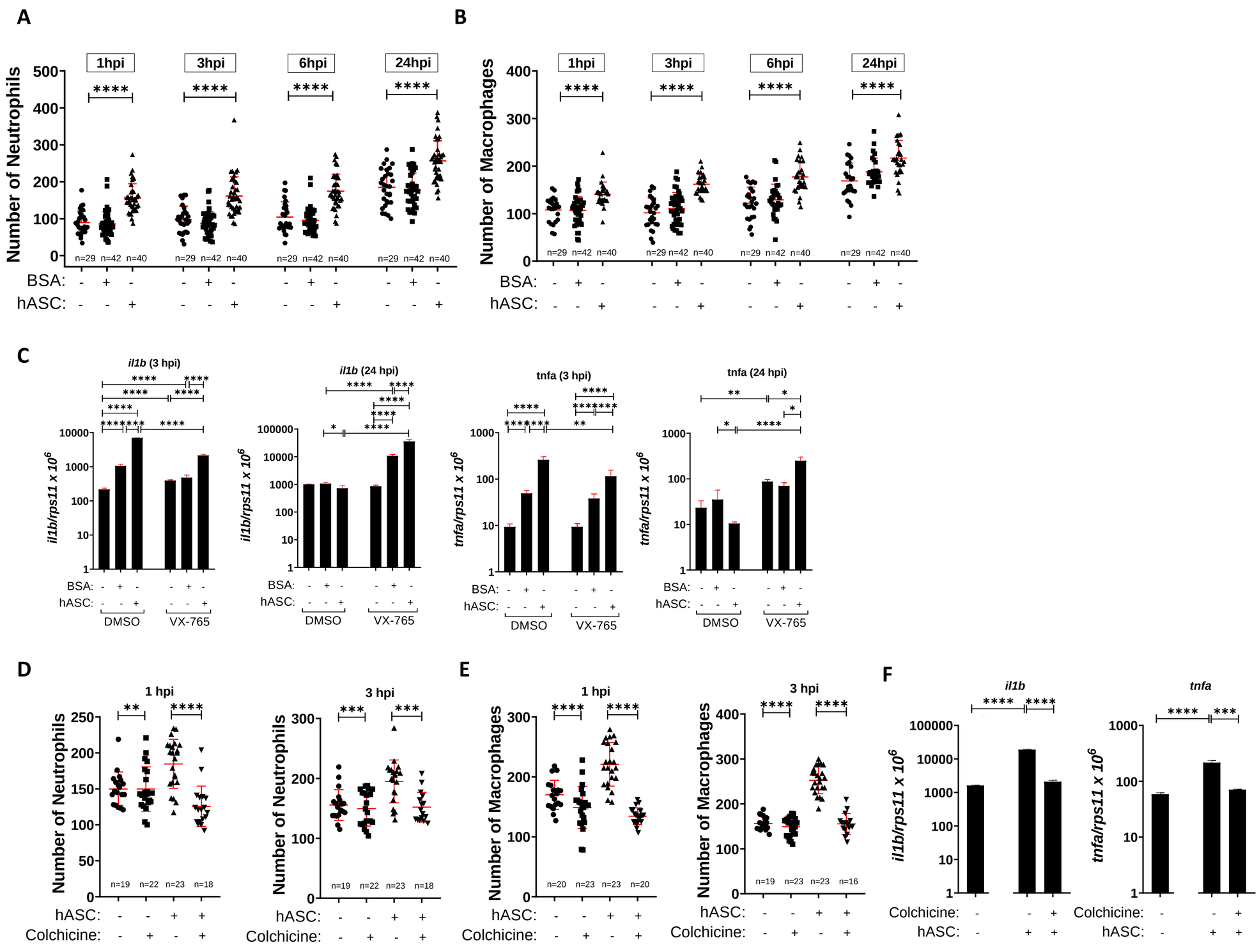

Figure 5. Extracellular ASC specks drive emergency myelopoiesis and hyperinflammation via inflammasome activation . hASC and BSA (as control) were injected in the pericardium of wild-type (C, F), *Tg(mpx:eGFP)* (A, D) and *Tg(mfap4:tomato)* (B, E) larvae. In some experiments larvae were treated by immersion with DMSO/water, as controls, or with a specific inhibitor of caspase-1 (VX-765, 100 µM) (C) or 1 mg/ml colchicine (D, E, F). The transcript levels of the indicated genes (C, F) were analyzed at 24 hpi by RT-qPCR. Neutrophil (A, D) and macrophage (B, E) number and their recruitment were analyzed at 1, 3, 6 and 24 hpi by fluorescence microscopy. Each dot represents one individual, and the means ± SEM for each group is also shown. P values were calculated using one-way analysis of variance (ANOVA) and Tukey multiple range test. *P ≤ 0.05, **P ≤ 0.01, ***P ≤ 0.001, and ****P ≤ 0.0001. auf, arbitrary units of fluorescence.

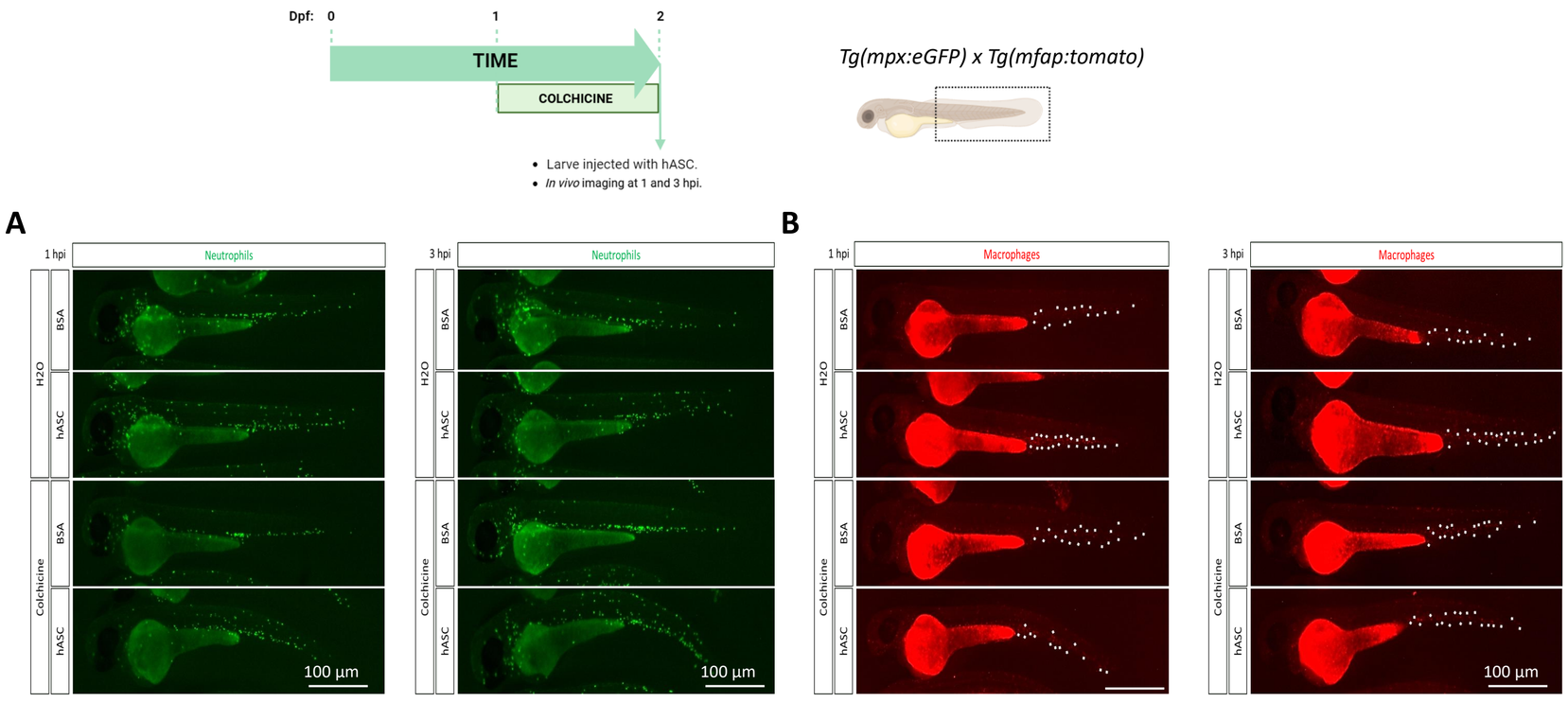

Figure S7 (related to Figure 5). Representative green and red fluorescence images of larvae of the different groups shown in Figures 5A, B, D, E. Two-dpf *Tg(mpx:eGFP)* (A) and *Tg(mfap4:tomato)* (B) larvae were injected in the pericardium with either hASC or BSA (control), then treated by immersion with 1 mg/ml colchicine. Neutrophil (A) and macrophage (B) number was analyzed by fluorescence microscopy at 1 and 3 hpi. The regions of interest used for quantification in all experiments are indicated in the schematic representation of the larvae. Bars: 100 µm (whole larva) and 50 µm (head).

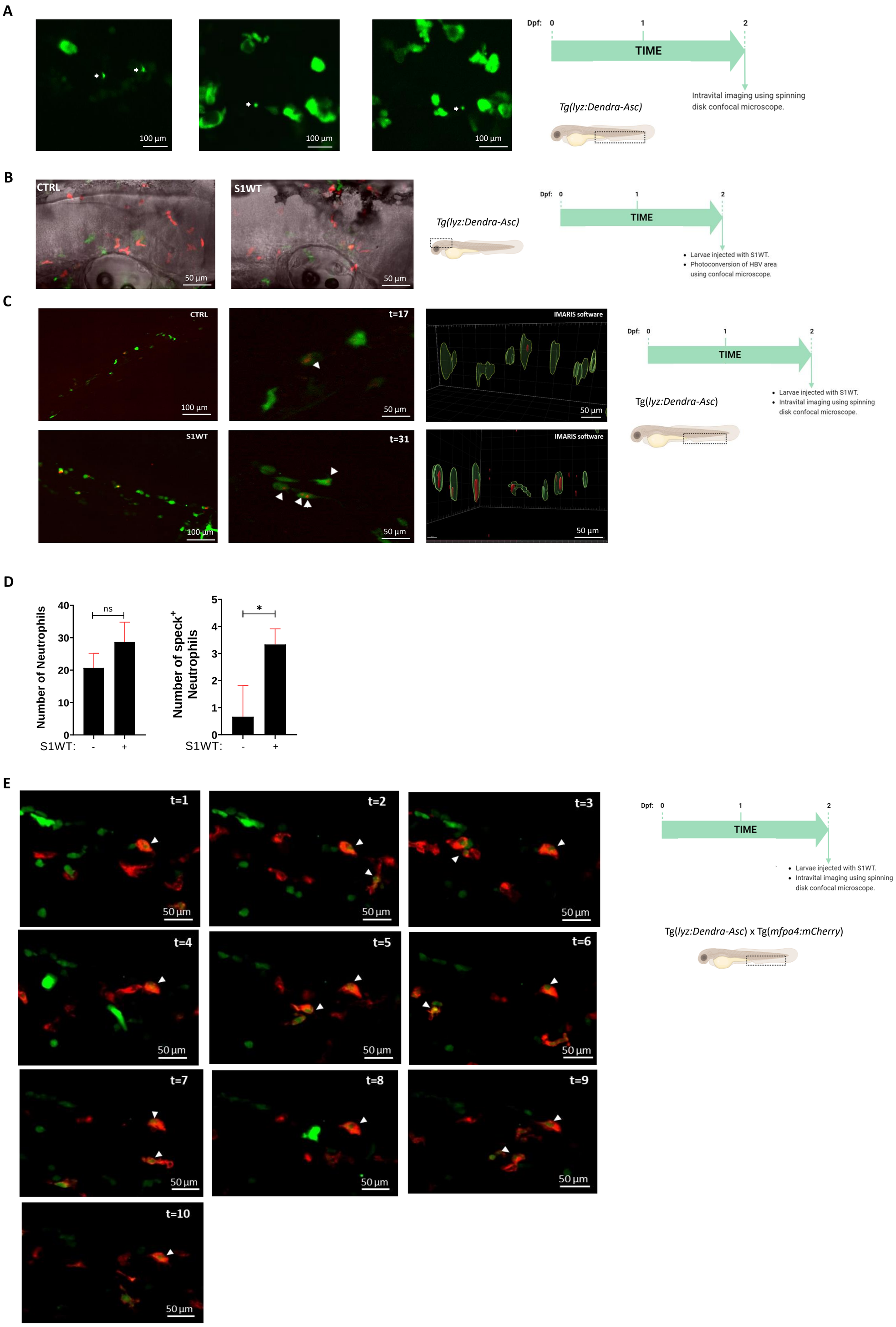

Figure 6. Neutrophil to macrophage Asc speck transfer occurs in vivo. High resolution intravital imaging of CHT was performed with the spinning disk to visualize in vivo Asc-speck formation in *Tg(lyz:Dendra-Asc*) larvae (A). Recombinant S1WT (+) or vehicle (−) were injected in the hindbrain ventricle (HBV) of 2 dpf Tg(lyz:Dendra-Asc) (B-E). HBV photoconversion of 2 dpf *Tg(lyz:Dendra-Asc)* larvae after S1WT injection, using LSM880 airyscan (B) and high resolution intravital imaging of CHT was performed with the spinning disk to visualize in vivo Asc-speck formation, release and spreading (in red). 3D IMARIS software was used for image analysis (C). Neutrophil (in green) (C, E) and Asc-speck (in red) (C) or macrophage (in red) (E) number were analyzed for 8 h during confocal spinning disk imaging. The total number of neutrophils and the number of neutrophils with speck in S1-injected larvae are shown (D). P values were calculated using Student´s t-test. *$P \leq 0.05$. The regions of interest used for quantification in all experiments are indicated in the schematic representation of the larvae. Bars: 100 µm (CHT area) and 50 µm (HBV).

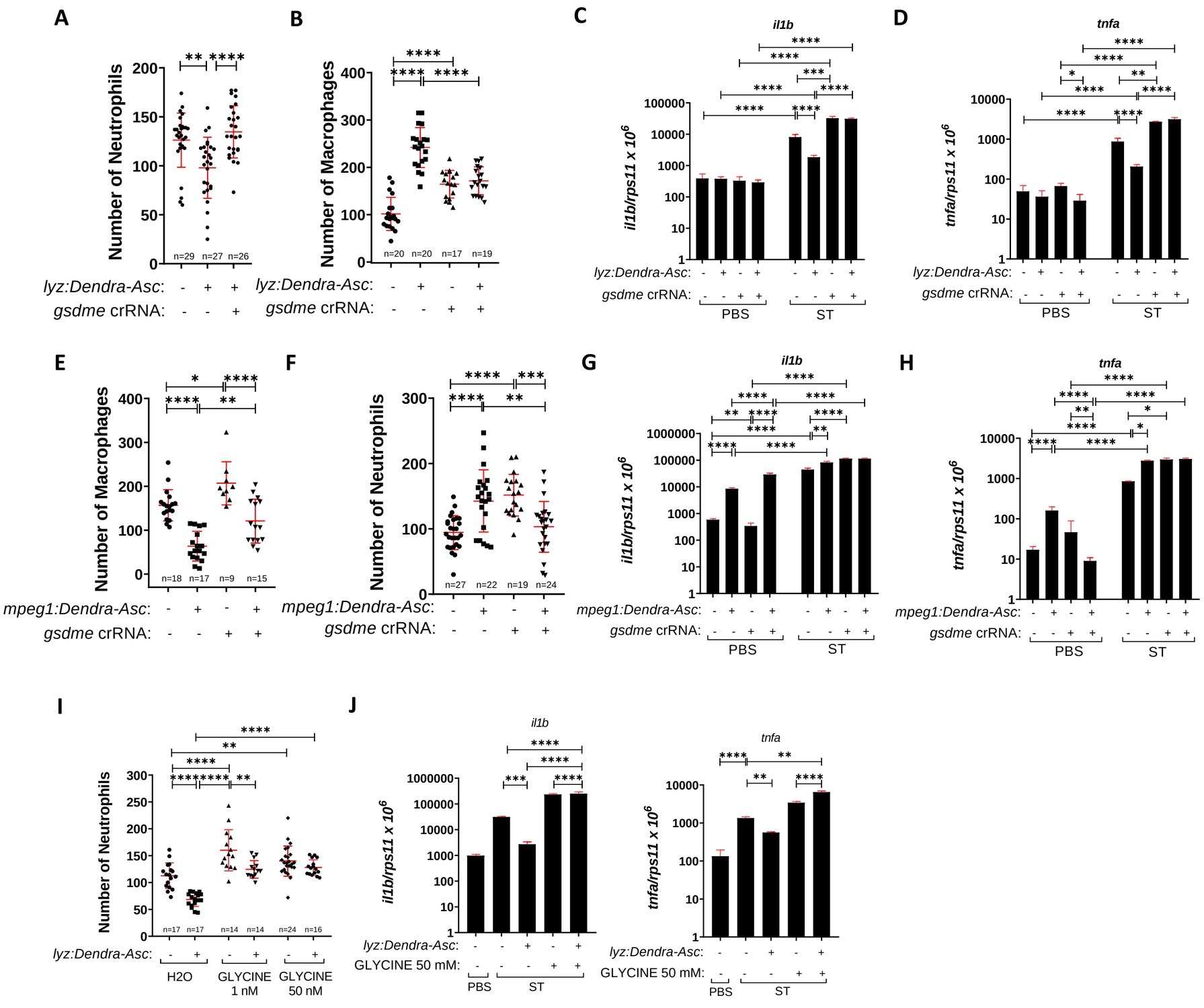

Figure 7. Gsdme- and Ninj1-driven cell death mediate the crosstalk between neutrophils and macrophages. Zebrafish one-cell embryos were injected with *gsdme* gRNA/Cas9 complexes (A-H) or/and with *mpeg1:Dendra-Asc* plasmid (E, F, G, H, K, L). ST was then injected in the yolk sac of 2 dpf *Tg(lyz:Dendra-Asc)* (C, D, J), and *mpeg1:Dendra-Asc* injected (G, H, L) larvae. Zebrafish larvae were also treated by immersion with DMSO or with the specific PMR inhibitor glycine (I, J, K, L). The transcript levels of the indicated genes (C, D, G, H, J, L) were analyzed at 24 hpi by RT-qPCR. Neutrophil (A, F, I) and macrophage (B, E, K) number was analyzed at 2 dpf by fluorescence microscopy. Each dot represents one individual, and the means ± SEM for each group is also shown. P values were calculated using one-way analysis of variance (ANOVA) and Tukey multiple range test. *P ≤ 0.05, **P ≤ 0.01, ***P ≤ 0.001, and ****P ≤ 0.0001.

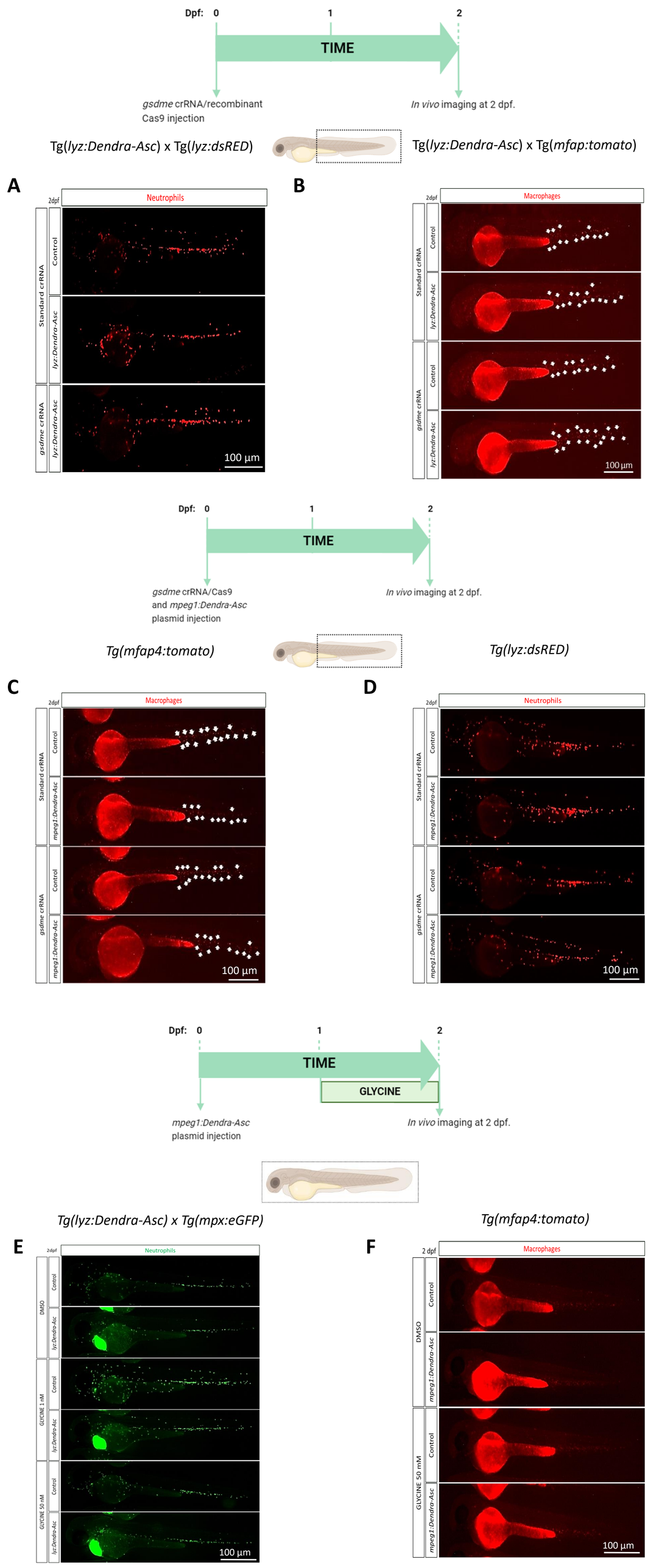

Figure S7 (related to Figure 7). Representative green and red fluorescence images of larvae of the different groups shown in Figure 7. Zebrafish one-cell embryos were injected with gsdme gRNA/Cas9 complexes (A-D) or/and with *mpeg1:Dendra-Asc* plasmid (C, D, F). Zebrafish larvae were also treated by immersion with DMSO or with the specific PMR inhibitor glycine (E, F). Neutrophils (A, D, E) and macrophages (B, C, F) in the body were visualized at 6 hpi by fluorescence microscopy. The regions of interest used for quantification in all experiments are indicated in the schematic representation of the larvae. Bars: 100 µm.

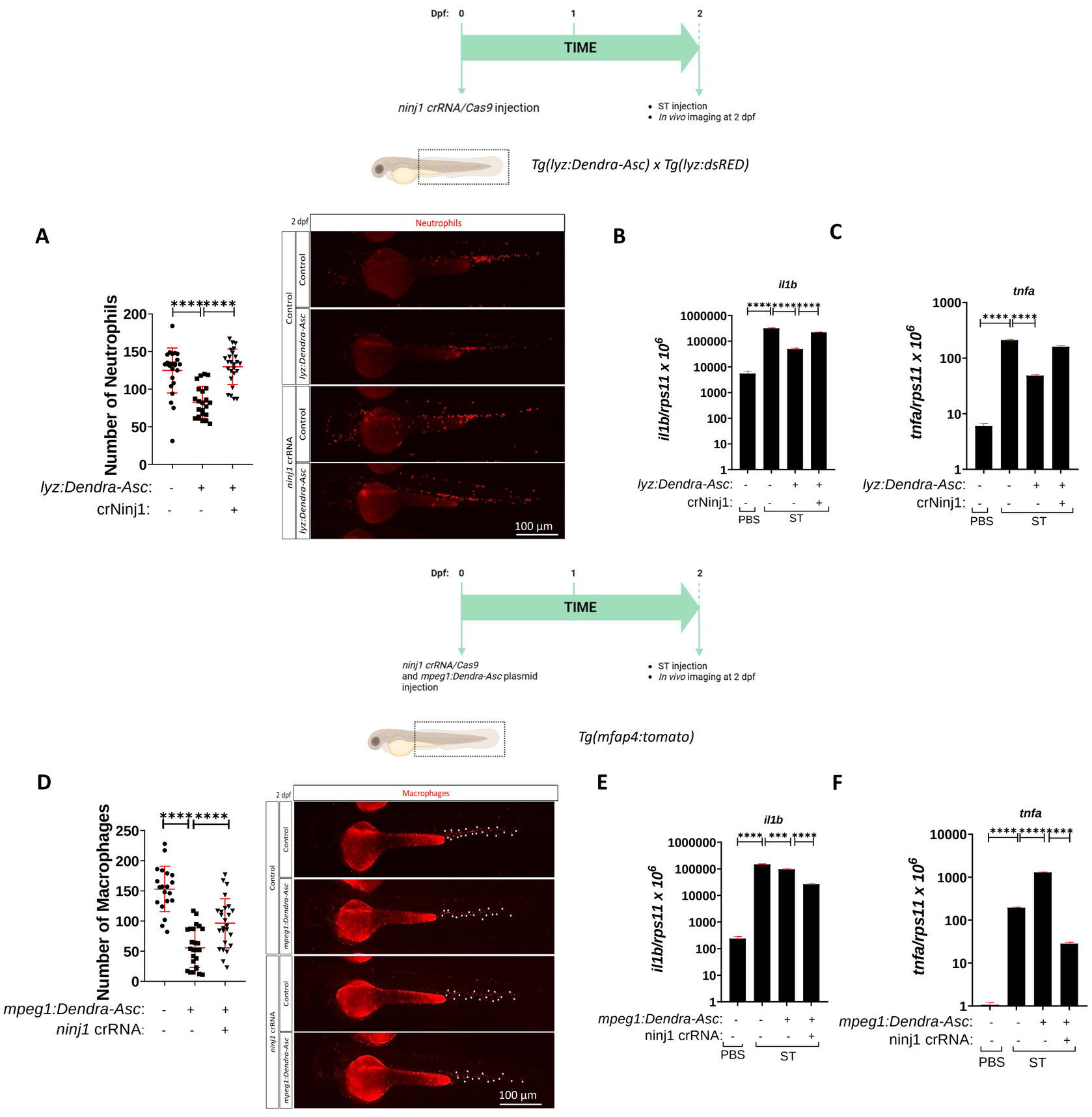

Figure S8 (related to Fig. 7). Ninj1-driven cell death mediate the crosstalk between neutrophils and macrophages. Zebrafish one-cell stage embryos were injected with *ninj1 g*RNA/Cas9 complexes (**A-F**) or with *mpeg1:Dendra-Asc* plasmid (**D, E, F**). At 2 dpf larvae were injected with ST in the yolk sac (**B**, **C**, **E**, **F**). Neutrophils (**A**) and macrophages (**D**) in the body were visualized at 6 hpi by fluorescent microscopy. The transcript levels of the indicated genes (**B**, **C**, **E, F**) were analyzed at 24 hpi by RT-qPCR. Each dot represents one individual, and the means ± SEM for each group is also shown. *P* values were calculated using one-way analysis of variance (ANOVA) and Tukey multiple range test. $^{**}P \leq 0.01$, $^{***}P \leq 0.001$, and $^{****}P \leq 0.0001$. The regions of interest used for quantification in all experiments are indicated in the schematic representation of the larvae. Bars: 100 µm.

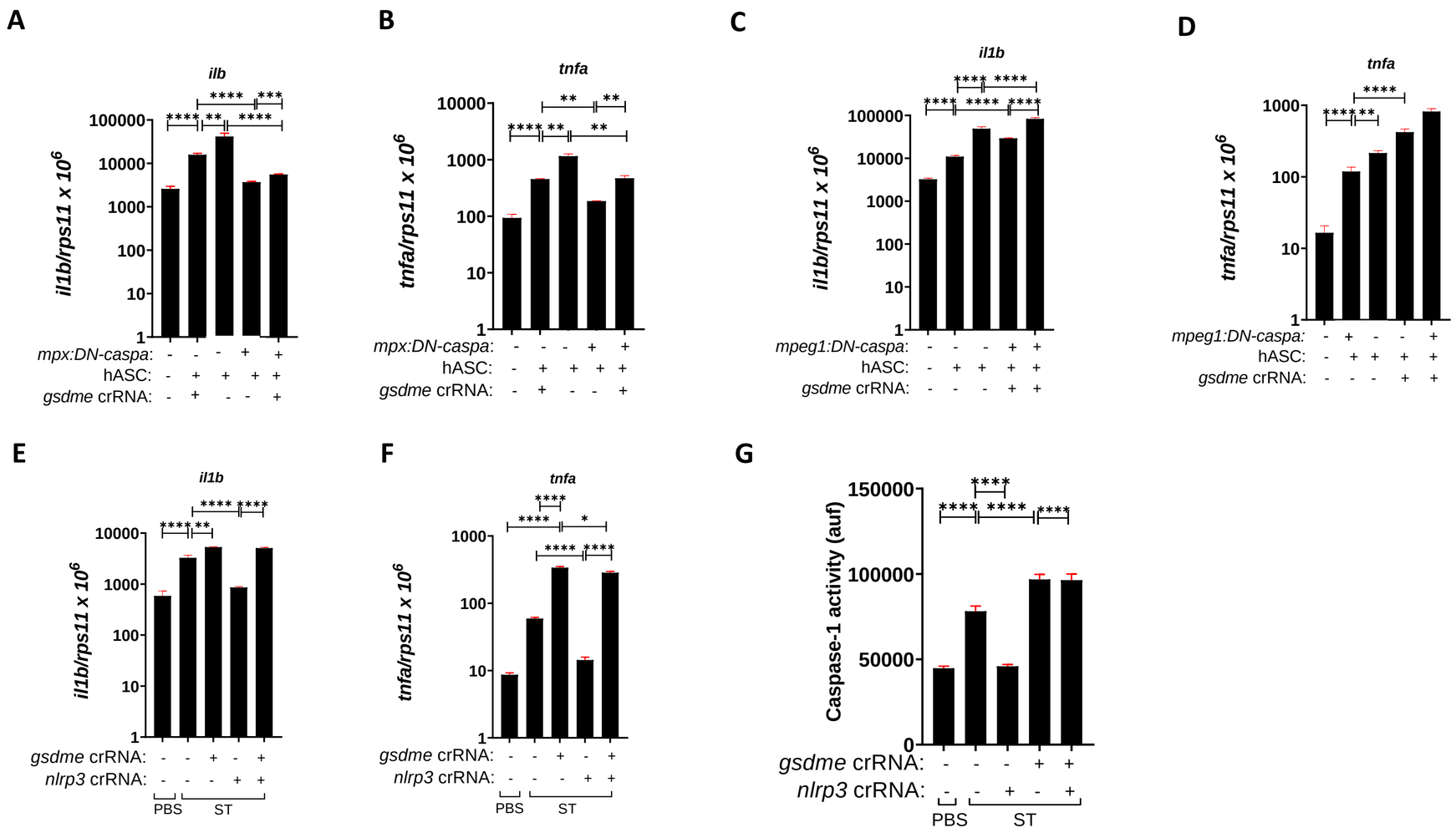

Figure S9 (related to Fig. 7). Gsdme drives the feedback inhibition of inflammasome activity in macrophages. Tg*(mpx:DN-caspa)* (**A, B**), Tg*(mpeg1:DN-caspa)* (**C, D**) embryos were used. Wild type (**E, F, G H**) one-cell stage embryos were injected with *gsdme* and/or *nlrp3 g*RNAs/Cas9 complexes (**E, F, G**). At 2 dpf hASC was injected in the pericardium (**A, B, C, D**). At 2 dpf larvae were injected with ST in the yolk sac (**E, F, G**). The transcript levels of the indicated genes (**A-F**) were analyzed at 3 or 24 hpi by RT-qPCR. Caspase-1 activity was determined at 24 hpi using a fluorogenic substrate (**G**). Each dot represents one individual, and the means ± SEM for each group is also shown. *P* values were calculated using one-way analysis of variance (ANOVA) and Tukey multiple range test. $^{**}P \leq 0.01$, $^{***}P \leq 0.001$, and $^{****}P \leq 0.0001$.

Table S1. gRNA used in this study. The gene symbols followed the Zebrafish Nomenclature Guidelines (http://zfin.org/zf_info/nomen.html).

Gene	Name	Sequence (5'→3')
gsdmea	CD.Cas9.PQCQ3167.AA	CATCCCACCGGACACTGTGT
gsdmeb	Dr.Cas9.DFNA5B.1.AO	GCAGACACGGAACGCAAAGA
nlrp3	CD.Cas9.BNQV6690.AA	GGACATCGTCCACTGAACTA
ninj1	CD.Cas9.VQMP9520.AA	GAATGGAGGTGTAAACCGAA

Table S2. Primers used in this study. The gene symbols followed the Zebrafish Nomenclature Guidelines (http://zfin.org/zf_info/nomen.html).

Gene (ENA or ENSEMBLE accession number	**Name**	**Sequence (5'→3')**	**Use**
rps11 (ENSDARG00000053058)	F	ACAGAAATGCCCCTTCACTG	RT-qPCR
	R	GCCTCTTCTCAAAACGGTTG	
il1b (ENSDARG00000098700)	F	GCCTGTGTGTTTGGGAATCT	
	R	TGATAAACCAACCGGGACA	
tnfa (ENSDARG00000009511)	F	GCGCTTTTCTGAATCCTACG	
	R	TGCCCAGTCTGTCTCCTTCT	
gsdmea (ENSDARG00000086762)	F	ACTGGACCTTAAACACTCTTTGAT	PCR
	R	ATACCGTCTGTCTGTCAGTGC	
gsdmeb (ENSDARG00000040485)	F	GCTGGATTTGCAGAAGCTCTTACATG	
	R	AACCACCCTTGCTTACAGCG	
nlrp3 (XM_017355939.2)	F	GGGGGAAGGACAAGGGAAAC	
	R	GACATTCCCTCCACCCTCAC	
ninj1 (ENSDARG00000103663)	F	TCCTGCAACGTTTCTTTTGCATC	
	R	CGACGCCCGCATAAAAGGAA	